

1

NOvA Test Beam detector calibration

2

Technical Note

3

Robert Kralik

University of Sussex

4

September 9, 2023

5

Abstract

6

What is this about and what will I describe in here

7

Contents

8	1	Introduction	3
9	2	Overview of the Test Beam detector	5
10	3	NOvA calibration process	8
11	3.1	Calibration samples	11
12	3.2	Fiber brightness	13
13	3.3	Threshold and shielding correction	13
14	3.4	Relative calibration	14
15	3.5	Absolute calibration	16
16	3.6	Calibration uncertainties	17
17	4	NOvA Test Beam detector calibration	18
18	4.1	Overview	18
19	4.1.1	Definitions	19
20	4.2	Detector Brightness	19
21	4.3	Threshold and shielding corrections	19
22	4.4	Simulation	19
23	4.4.1	Relative calibration results	20
24	4.5	Period 1	20
25	4.6	Period 2	20
26	4.6.1	Relative calibration results	20
27	4.7	Period 3	20
28	4.7.1	Relative calibration results	27
29	4.8	Period 4	27
30	4.8.1	Relative calibration results	27

31	4.9 Absolute calibration results	27
32	4.10 Drift in TB data	30
33	4.11 Results	30
34	4.12 Validation	30

35 1 Introduction

36 TO DO:

- 37 • Divide the motivation to abstract (why do we care about test beam calibration, what did**
- 38 we do and how did we do it. What are the results)**
- 39 • and introduction (brief history of test beam calibration, maybe a bit more detail into why**
- 40 is test beam calibration important)**

41 Why is Test Beam? "The idea, as with any test beam experiment, is to expose a detector
42 to a beam of very well-characterized particles, so that we can improve our understanding of
43 how the detector responds to such particles. We make use of upstream detectors to collect
44 data on the beam particles before they interact in the NOvA detector. For example, we will
45 be able to see what a 1 GeV proton actually looks like in our detector, without having to
46 simulate it, and we can test how well we would have reconstructed the energy using our existing
47 techniques. We may find we are able to make improvements to our tools to better match what
48 we see in the detector with how we reconstruct it. Or we may find we already do a pretty
49 good job. Either way, with a full cross-comparison like this, we can be more confident in our
50 analysis of the data and reduce the level of uncertainty we consider are associated with the
51 relevant measured quantities. Ultimately, the aim will be to reduce the level of uncertainty on
52 the neutrino oscillation analyses and to make even better, more accurate measurements of the
53 Standard Model."Why is Test Beam calibration done:

- 54 • To be able to directly compare TB to the standard detectors**
- 55 • To be able to verify our calibration procedures using TB data**
- 56 • To study the particle response as a function of energy**
- 57 • To determine an energy resolution**
- 58 • To compare currently used energy scales to data and understand if we can use TB data**
59 for absolute energy scale in all NOvA detectors

60 For DeltaM2: By increasing exposure, total syst. error decreases by (+) 18.5For sin2Th23:
61 Difference by reducing calib syst.: (+) 10.8Statement: "The NOvA Test Beam will improve
62 the total systematic error on the final measurement of the oscillation parameters Dm232 and
63 sin2Th23 by 10Potential Test Beam impacts: Check modeling of hadronic interactions in de-
64 tector (check GEANT systematics), Using Test Beam data as "single-particle MC" to train
65 CNN prong-like algorithms, Generate Adversarial Networks for MC improvements using
66 Test Beam data, Check ND calibration procedure to try and understand causes of 3-5

- 67 • Hadronic response and comparison with MC modeling**
 - 68 – response as a function of energy**
 - 69 – establishing of an absolute energy scale**
 - 70 – determination of energy resolution**
 - 71 – studies of topological features and resolution**

- 72 * pion tracking and showers
73 * proton tracking and showers
74 – studies of timing features and resolution
75 • Electromagnetic response and comparison with MC modeling
76 – response as a function of energy
77 – establishing of an absolute energy scale
78 – determination of energy resolution
79 – studies of topological features and resolution
80 * electron signatures
81 * gamma signatures
82 – studies of timing features and resolution
83 – studies of π^0 from π^- charge-exchange
84 • Muon response and comparison with MC modeling
85 – comparison with detailed optical simulations
86 – determination of energy resolution
87 – studies of topological features and resolution
88 – cross-talk studies
89 – comparison to cosmic ray muons (requires a special trigger)
90 – studies of the muon calibration protocol
91 • Light yield and response studies as a function of particle type and detector configuration
92 – understanding the Cherenkov light contribution
93 – vertical and horizontal responses and comparison with simulations
94 – data with selected planes rotated by 45 and 90 degrees
95 – slanted (angle) plane response (and subset of programs as above)
96 – fiber attenuation studies
97 – Birks' constant studies
98 • Near / Far readout comparison
99 • Gather large libraries of particles at known energies and multiple angles of incidence to
100 help develop a CNN prong ID. Also allows training of a particle-based CVN-like PID.
101 Also use information from:
102 • NOvA Test Beam Technical Statement of Work
103 • NOvA Test Beam program (paper for DOE) [docdb:25074]

- 104 • NOvA Test Beam task force report [docdb:15750]
 105 • Overview presentation of NOvA Test Beam [docdb:20495]
 106 • Test Beam support document [docdb:22172]
 107 • NOvA Test Beam program proceedings [docdb:55808]
 108 Mike's proceedings from ICHEP 2020 [?].

109 2 Overview of the Test Beam detector

110 The NOvA Test Beam detector is a scaled down version of the Near and Far Detectors shown
 111 on figure 1. It is placed in the MC7b enclosure of the Fermilab Test Beam Facility in the path
 112 of the MCcenter beamline with a variety of beamline detectors to measure and identify a range
 113 of particles with various momenta [?].

114 Maybe also mention the specific times Test Beam detector was operational.

115 Majority of the Test Beam detector and it's instrumentation is identical to the other NOvA
 116 detectors, but there are a few differences, including size, scintillator oil used, readout electron-
 117 ics, or environmental controls, that we're discussing in this section.

118 Should I aslo talk about the beam halo? Could that have an influence on the calibration?

119 Maybe it's the peaks in the cosz distribution?

120 General parameters

121 The NOvA Test Beam detector consists of two 31-plane blocks, each beginning and ending
 122 with a vertical plane, with an additional horizontal plane glued inbetween them to preserve the
 123 alternating arrangement [?]. Each plane consists of 2 modules side-by-side and each module is
 124 made up of 32 cells. Each cell has an inner (without the PVC) depth and width of 5.9 cm and
 125 3.8 cm respectively, same as for the other NOvA detectors, and a length of 2.6 m. This brings
 126 the final dimensions of the Test Beam detector to 63 planes \times 64 cells, or $2.6 \times 2.6 \times 4.1 \text{ m}^3$.

127 The 63 planes are numbered from 0 to 62, with even numbers corresponding to vertical
 128 planes and odd numbers to horizontal planes. Cells are numbered 0 to 63, going from bottom
 129 to top for horizontal planes and left to right, when facing the front of the detector, for vertical
 130 planes.

131 The detector coordinate system is illustrated on figure 1. It is centered with $(0, 0, 0)$ in the
 132 centre of the first plane [?]. The x axis runs left to right when facing the front of the detector,
 133 y axis bottom to top, and z axis goes along the beam direction from front to the back of the
 134 detector. The exact geometry of the Test Beam detector from several alignment surveys is saved
 135 in gdml files and used in our analyses [?].

136 In the past we encountered an issue when aligning the Test Beam detector with the beamline
 137 measurements broke several assumptions within the Test Beam geometry [?], which manifested
 138 as uncalibrated cells in the back of the detector [?]. This was fixed by realigning both the
 139 detector and the beamline based on the last alignment survey and implemented in the production
 140 tag R23-04-05-testbeam-production.a and there after [?].

141 Should I define w here? And tehn mention it in the readout section to say that readout is
 142 always on the positive side of the detector. Additionally we use the coordinates measured by

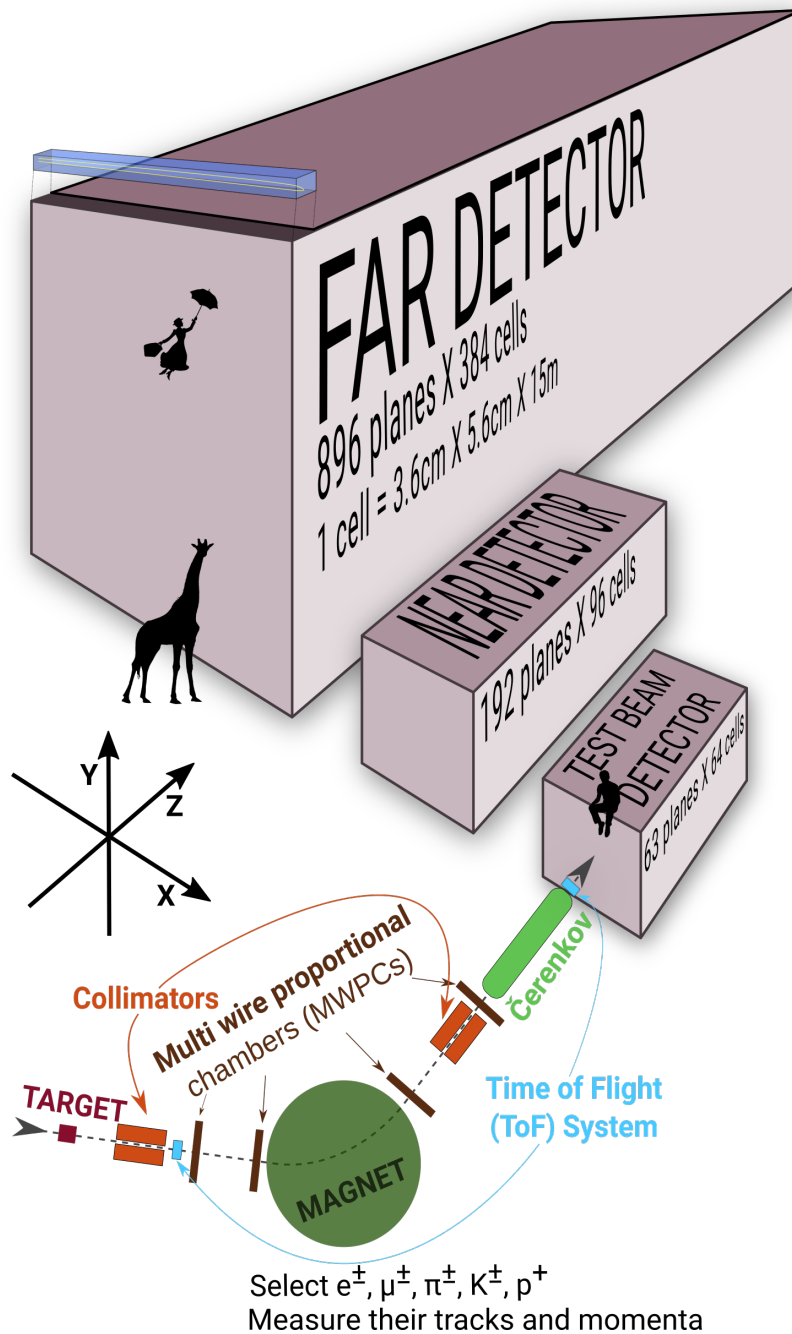


Figure 1: Comparison of Test Beam detector scale to the Near and Far NOvA detectors (and a man, giraffe, or Mary Poppins). Also shown are the Test Beam beamline detectors and components (not to scale), with arrows showing the direction of the beam. The three black arrows show the orientation fo the detector coordinate system.

- ¹⁴³ cell number V and the distance along the cell length W independent of the view in question.
- ¹⁴⁴ Extensive use of W is made throughout this document and the code. Note: W is not the distance
- ¹⁴⁵ to the readout, it is simply an alias for x or y, so W = 0 is at the cente of detector. It happens that
- ¹⁴⁶ the readout and coordinate system are arranged such that more positive values of W are closer
- ¹⁴⁷ to the readout. [docdb:13579 - SA The Attenuation and Threshold Calibration of the NOvA

148 detector]

149 Scintillator

150 The Test Beam detector is filled with (more than) three different versions of the NOvA scin-
151 tillator, which differ mainly in the way they were stored since the filling of the near and far
152 detectors. This is illustrated on figure 2.

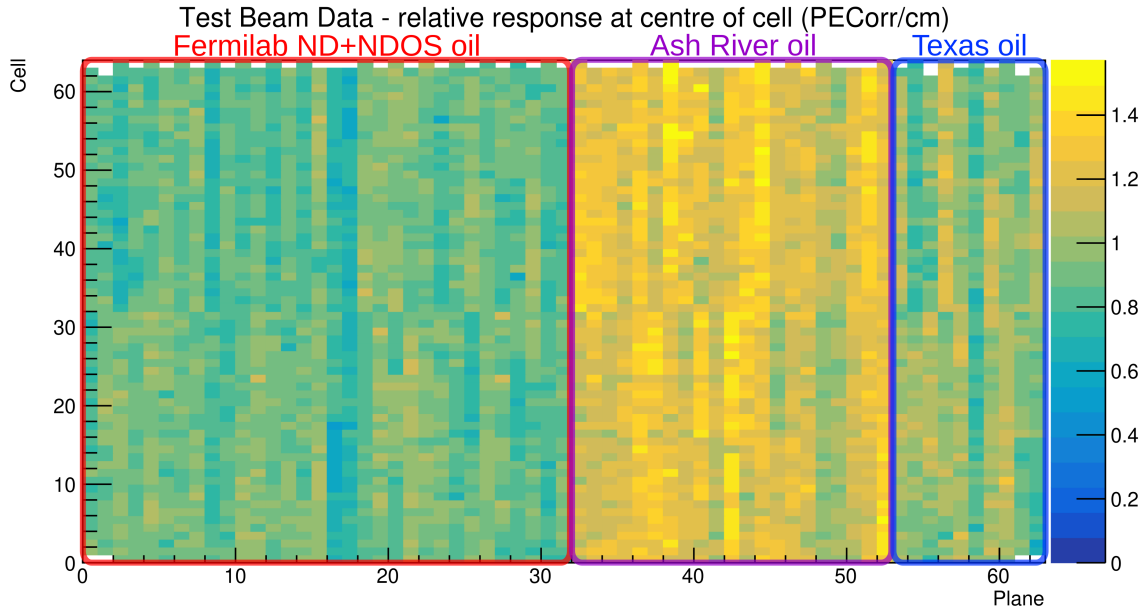


Figure 2: Uncorrected energy response in the centre of cells across the Test Beam detector showing a clear distinction between the different scintillator oils.

153 The original plan [?] was to use the scintillator from a tanker and one of the tanks located
154 outside in Fermilab. First tests showed acceptable results and the tanker oil was used to fill out
155 almost the entirety of the first block of the detector (first 32 planes) [?]. However, when we
156 loaded the oil from tank two into the tanker, it became extremely cloudy and unusable, possibly
157 due to contamination with water accumulated at the bottom of the tanks, which was mixed with
158 oil by the pump. The rest of the first block was topped up with high quality scintillator
159 from NDOS, which has been stored inside in barelles at MiniBooNE [?]. This is labeled as
160 "Fermilab ND+NDOS oil" on figure 2.

161 Even before the extreme cloudiness was discovered, it was known that the oil from the tanks
162 has lost much of its original light yield properties. Reasons vary from water contamination to
163 insects and dirt contamination [?]. Yet it was still decided to use the tank 2 oil [?]. It was
164 also decided not to mix the various oils (tanker/tank/NDOS/Ash River) as studying energy
165 deposition in different types of oils could lead to some interesting insights [?].

166 The first 21 planes of the second block (planes 32 to 52) were filled with the Far Detector
167 production scintillator shipped in from Ash River [?]. This oil has been stored in "totes" inside a
168 building and under several layers of black plastic [?]. Also used a little (70 gallons) scintillator
169 from NDOS to fill these planes (compared to 1900 gallons from Ash River) [?].

170 The last 10 planes (planes 53 to 62) [?] were filled with scintillator drained from NDOS
171 stored in Texas A&M University and University of Texas at Austin [?, ?]. This scintillator has

¹⁷² higher light yield than the one from the tanker, but lower than the Ash River one [?].

¹⁷³ In total the Test Beam detector is filled with 5418 gallons of scintillator oil with a weight
¹⁷⁴ of approximately 28.6 tons [?].

¹⁷⁵ **Readout**

¹⁷⁶ The Test Beam detector uses in total 126 front end boards (FEBs), each reading out signal from
¹⁷⁷ 32 cells (half of a plane) [?]. The readout is located on the top and right (looking on the front)
¹⁷⁸ side of the detector. 118 FEBs are version 4.1, same as in the Far Detector, and 8 FEBs, located
¹⁷⁹ on planes 16, 17, 48 and 49, are version 5.2, same as in the Near Detector. The Near Detector
¹⁸⁰ FEBs are designed to read out data in a faster rate and we used a mix of FEB types to study the
¹⁸¹ difference in their response and to validate both versions in the same environment [?].

¹⁸² **Environment**

¹⁸³ Unlike the near and the far detector, the Test Beam detector does not have any overburden to
¹⁸⁴ shield it from cosmic particles.

¹⁸⁵ Temperature very stable during winter months (heCng is installed at MC7). However, dew
¹⁸⁶ point went over 10C ND shutdown threshold several times.

¹⁸⁷ **Underfilled cells issue**

¹⁸⁸ The Test Beam detector is slightly tilted around the Z axis by about 0.7° towards the readout.
¹⁸⁹ This caused the top cells of both modules of all the horizontal planes (cells 31 and 63) to be
¹⁹⁰ underfilled, creating an air bubble on the left side of the detector and severely affecting the
¹⁹¹ energy response in those cells [?]. This has been fixed [?] by adding extensions to the filling
¹⁹² ports and overfilling the horizontal cells with the NDOS scintillator stored in drums Fermilab
¹⁹³ (not the scintillator store in a tanker or tanks). This scintillator was also used in the first half
¹⁹⁴ of the detector (Fermilab ND+NDOS oil on figure 2), but is different from the "Ash River oil"
¹⁹⁵ used in part of the second half of the detector (bright part of figure 2). The overfilling was done
¹⁹⁶ in April 2021 in 3 stages in between the full operation of the Test Beam detector.

¹⁹⁷ **3 NOvA calibration process**

¹⁹⁸ Test Beam is intentionally following the same calibration procedures as the standard NOvA
¹⁹⁹ detectors. This section intends to provide a brief overview of the general NOvA calibration
²⁰⁰ process and introduce basic utilities used.

²⁰¹ This is all done inside the NOvAsoft Calibration package and applied with the Calibrator
²⁰² package.

²⁰³ Describe that the results of the calibration process are stored in csv tables and loaded during
²⁰⁴ processing of each event.

²⁰⁵ Give links to other calibration technotes so that people can go take a look if they want more
²⁰⁶ information. This should be just a general overview, stating the facts, no really describing how
²⁰⁷ we got to where we are.

²⁰⁸ Should I talk about the timing calibration? It's applied when making the RecoHit, so at the
²⁰⁹ same time as applying the Calibration results

210 The purpose of calibration is to express the same amount of energy deposited anywhere
 211 inside any of NOvA's detectors at any time in the equal amount of energy in terms of physical
 212 units (MeV). NOvA uses cosmic ray muons, which provide a consistent and well understood
 213 source of energy deposition. [docdb:7410] Test Beam is following the same calibration proce-
 214 dures as the other NOvA detectors shown as a flow chart on figure 5. This section intends to
 215 provide only a brief overview of the NOvA calibration process and further details can be found
 216 in the other NOvA calibration technical notes [docdb:13579].

217 Cosmic muons are basically free to use and we're using stopping muons for the absolute
 218 calibration.

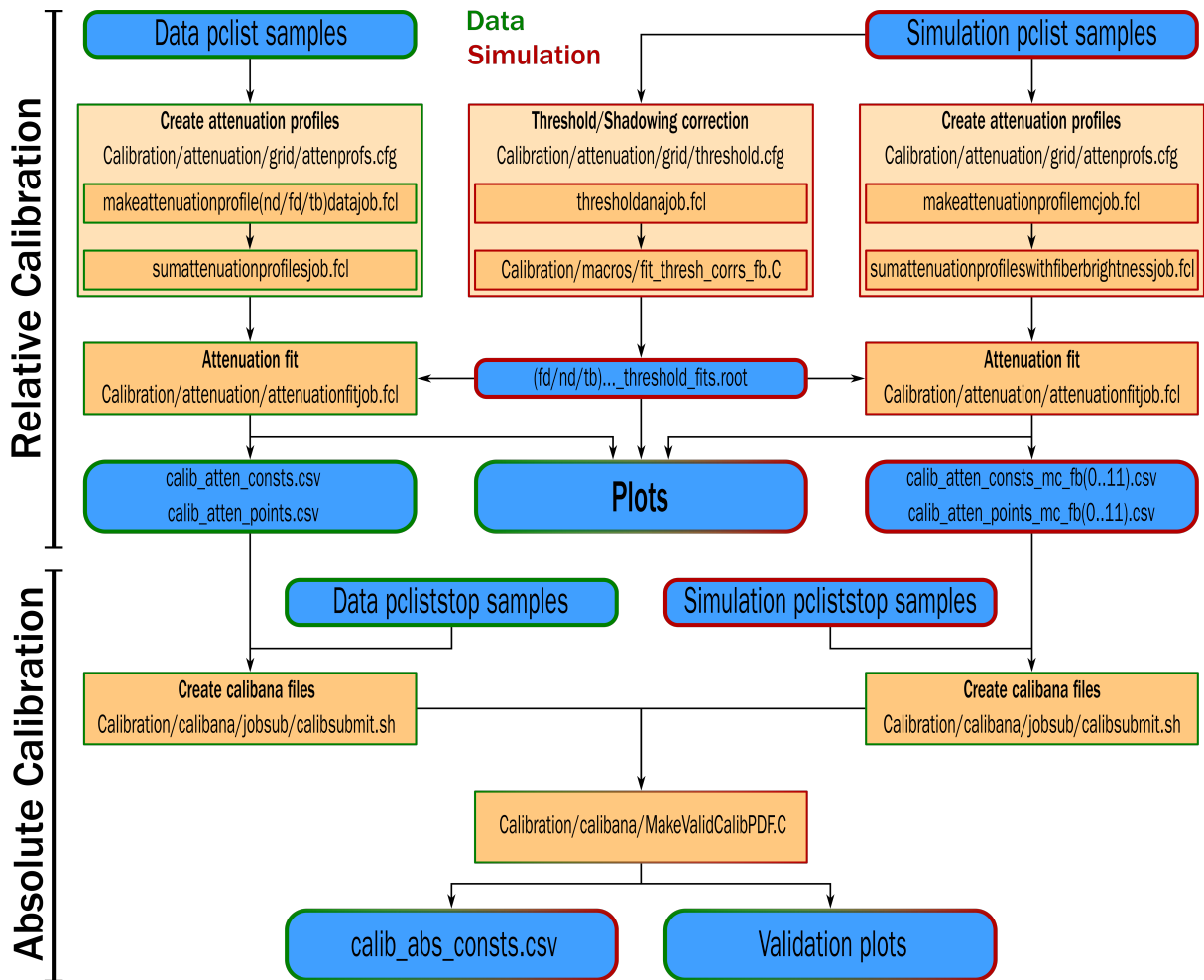


Figure 3: Flow chart showing the jobs (orange background) and files (blue background) needed and produced during the full NOvA calibration process. The left chain is showing the data calibration process (with green border) and is applied to every data calibration sample separately (periods or epochs). The center and right chains are showing the simulation calibration process (red border), which is redone only if there's a change to the detector simulation. The absolute calibration at the bottom combines data and simulation. The entire process is done separately for each NOvA detector.

219 Maybe talk about timing calibration and drift which is not really implemented yet. Or talk
 220 about it when talking about dividing data into epochs...

Calibration is necessary to convert electronic signals to physically meaningful energy in units of GeV. Two calibration steps precede the calorimetric energy calibration. First raw ADCs (Analogue Digital Conversion) are converted to units of photo-electrons (PE) using the known average response of the APDs; secondly an attenuation calibration corrects for the position dependent response [6]. A drift calibration may be included in the future to correct for changes in detector response over time. The calorimetric energy scale calibration is the last step in the calibration chain and the detector response should already be uniform in space and eventually also in time. [docdb:13579 - FA_Calorimetric_energy_scale]

For the near and far detectors calibration is performed separately for the relative calibration and for the absolute calibration.

General variables used to define the energy in NOvA are (most from docdb:13579 - SA The Attenuation and Threshold Calibration of the NOvA detector, copied from docdb:7410):

ADC	The peak value from the Analog to Digital Converter representing the charge collected by the APDs. This is in RawDigit
PE	Number of Photo Electrons. A simple rescaling of the best estimate of the peak ADC, which only depends on the FEB type and the APD gain settings. Done inside the Calibrator package. This is in CellHit and serves as the input for calibration.
PECorr	Corrected PE after applying the relative calibration. This value should be the same across and within all the cells in a detector. This is in RecoHit
MEU	Muon Energy Unit is the mean detector response per cm to a stopping muon tri-cell hit within the track window. Mean MeV/cm or mean PECorr/cm
MeV	Estimated energy deposited in the scintillator calculated from PECorr using the results of the absolute calibration. Additional correction for dead material needs to be made in order to get a calorimetric energy estimate. This is in RecoHit

Table 1: Definitions of variables commonly used in calibration.

$$E_{deposited}[\text{MeV}] = \underbrace{\frac{\text{MEU}_{truth}[\text{MeV}/\text{cm}]}{\text{MEU}_{reco}[\text{PECorr}/\text{cm}]}}_{\text{Absolute calibration}} \times \underbrace{\frac{\text{Average response}[PECorr]}{\text{Fitted response}[PE]}}_{\text{Relative calibration}} \times E_{deposited}[\text{PE}]$$

(Detector, epoch) (Detector, epoch, plane, cell, w)

3.1 Calibration samples

To select cosmic muons for calibration we first remove beam related events based on their time stamp relative to the beam spill as shown on figure ???. Then we reconstruct and select events based on their track and spill properties (reference?). Since we require a precise pathlength information we only selection so called *tri-cell* hits, i.e. we require that all accepted hits also have a recorded hit in both neighboring cells of the same plane, as shown on figure ???. In case there's a bad channel in a neighboring cell, we ignore this channel and look one cell further.

Explain the tricell condition and the xy, z and avg sample more here.

242 How do we create the calibration samples and what cuts are applied?

243 The first step in the attenuation calibration is to select the suitable hits from tracks of cosmic
244 ray muons. Because a reliable estimate of pathlength is required, not all hits are suitable for
245 use. If a cell has each of its neighbors in the same plane hit, then we know, for a Y view cell,
246 that the track entered through the upper wall, and exited through the lower wall. The pathlength
247 then is just the width of the cell divided by the direction cosine. This selection also significantly
248 decreases the chance that the hit in question is a noise hit. Allowance is made for neighboring
249 dead cells, so e.g. “hit, dead, hit, hit” would still lead the 3rd cell to be selected. The second best
250 hit selection, in cases where there are too many dead neighboring cells on each side, is the so-
251 called “z” estimator, where a hit is required at the same cell number in each of the neighboring
252 planes in the same view. The pathlength is then the ratio of cell depth to cz. [docdb:13579 - SA
253 The Attenuation and Threshold Calibration of the NOvA detector, copied from docdb:7410]

254 I should mention that the division into xy hits, z hits and avg hits is already done when
255 creating the calibration samples...

256 (Dividing data into periods and epochs) A new period is started for a major change to run-
257 ning conditions such as a horn current change, a long shutdown, target replacement, etc. Peri-
258 ods are divided into epochs. A new epoch is started whenever analysis or production reasons
259 dictate. Calibration has been performed for all the periods separately and has used the data that
260 are determined by the Data Quality group to be good. The effects of aging, temperature, partial
261 filling, and cooling are neglected. The drift calibration should be able to account for all of these
262 (but drift calibration doesn't really exist yet afaik). [docdb:13579 - SA The Attenuation and
263 Threshold Calibration of the NOvA detector]

264 from docdb:7410 A requirement that the track be “throughgoing” (lowest endpoint outside
265 the fiducial volume) was applied, but doesn't make much difference. I think this selection was
266 broken by the recent changes to StopperSelection anyway. (So it seems that it was required
267 for the relative calibration that the muons are through-going, but I assume this was discarded
268 somewhere down the line

269 from Calibration_Meta_READFIRST.pdf plist = list of pre-calibrated hist; these have a
270 position and PE count pliststop = plist files only containing events that look like stopping
271 muons

272 Mention exactly the name and the location of the fcl files to create the TB plist/ppliststop
273 files. (Or should I only do this in the next section when mentioning the TB calibration?)

274 What are the main variables that are in the calibration samples? Specifically the PE and
275 such.

276 When should I talk about the ADC to PE conversion? Here?

277 Tricell condition

278 Adding the underfilled cells to the bad channels which are automatically skipped for the tricell
279 condition

280 Stopping muon selection (from docdb:13579 - FA_Calorimetric_energy_scale) There are
281 two avenues for selecting stopping muons; i) selecting tracks whose reconstructed end point is
282 contained within the detector and ii) selecting tracks that have a Michel electron at one end.
283 Michel electrons are useful for both identifying muons and effective tagging of the end point of
284 muon tracks. The stopping selection requires the reconstructed end point of the muon track to
285 be at least 50 cm from the detector edge. The identification of a Michel electron at the end of a

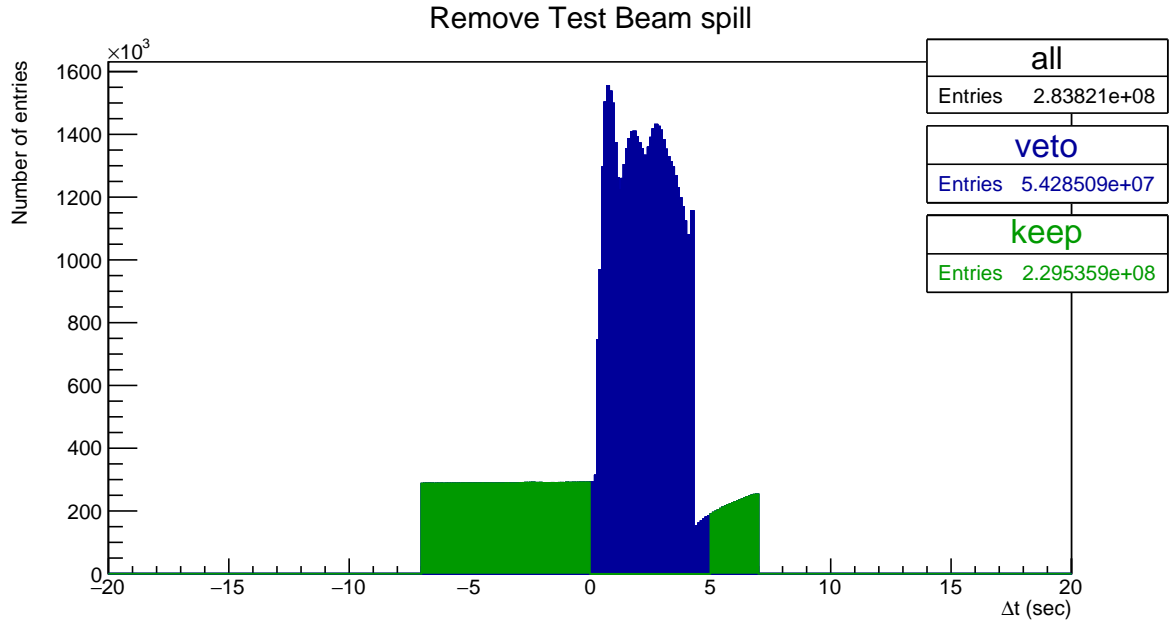


Figure 4: Test Beam beam spill events removed from the calibration samples. Test Beam beam spill is 4.2 seconds long and we remove events (in blue) within a 5 seconds window from the start of the beam spill. The remaining events (green) should mostly consist of cosmic particles. This example and the numbers of entries are for the full period 4 Test Beam sample.

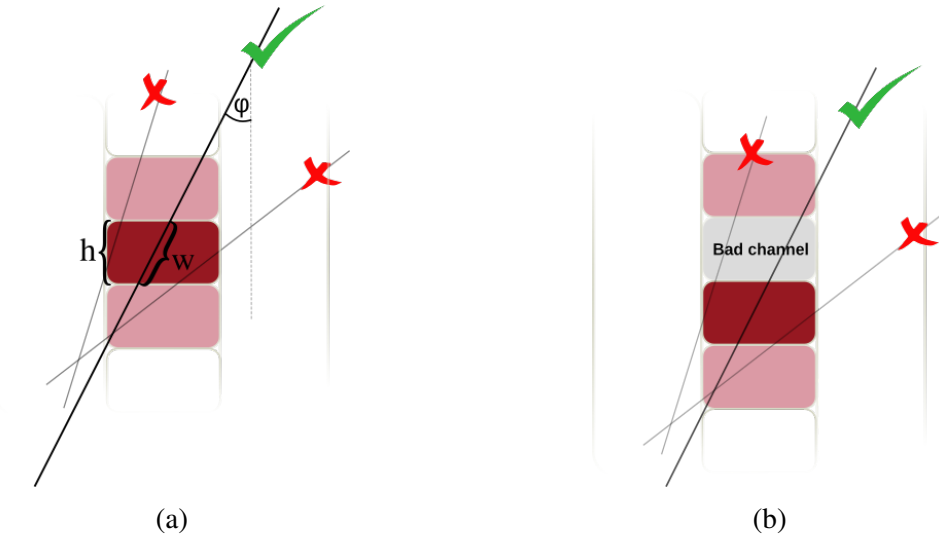


Figure 5: Illustration of the tricell condition (a). We only use hits that have two surrounding hits in the same plane to be used in the NOvA calibration. This is to ensure a good quality of the pathlength (w) reconstruction, which is calculated from the known cell height (h) and the reconstructed track angle (ϕ). In case the hit is next to a bad channel (b), we ignore this bad channel and require a hit in the next cell over.

muon track has two stages of both temporal and spatial range requirements. Firstly, a candidate Michel electron hit is required to occur between 1 and 30 microseconds after the mean time of the hits on the track. Furthermore, the candidate Michel electron must be within a 30 cm sphere surrounding the reconstructed track end point. The candidate Michel electron hit for a muon track is the hit that produces the largest detector response among the hits that pass the above cuts. Secondly, cell hits surrounding the candidate Michel electron hit are associated with the Michel electron if they occur within a 30 cm sphere surrounding the Michel electron candidate. Furthermore, to be associated with the Michel electron the cell hits must occur between 0.5 microseconds before and 0.5 microseconds after the candidate Michel electron. Michel electrons at the end of muon tracks are reconstructed using the candidate and associated Michel electron hits. The stopping muon selection requires a Michel electron at the end of the muon track.

3.2 Fiber brightness

Talk about fiber brightness, what it is and why do we have 12 fb bins and how do we get them now. Why are we doing a consolidated planes for simulation.

In the case of both Far and Near Detector Monte Carlo instead of hits being collated by plane and cell they are collated by view and cell. We pursue this strategy because our Monte Carlo cosmic sample is much smaller than the data, and because we can assume that the Monte Carlo detector is approximately uniform plane to plane. [docdb:13579 - SA The Attenuation and Threshold Calibration of the NOvA detector]

3.3 Threshold and shielding correction

Apply the threshold/shielding correction.

In the Far Detector data and MC a large divergence between calibrated and true energies as a function of W was observed [8]. This was traced back to the much longer cell lengths in the FD meaning that thresholds play a large role at the foot of a cell. Also self-shielding of the detector by its own mass lay a role in the observed discrepancy. Thresholds mean that for a hit to be seen by an APD, it may need to have a slight upwards fluctuation in the number of photons produced by the energy deposition. Self-shielding means that the average visible energy depositions from MIPs are not truly spatially uniform in the detector. If not corrected for these effects, there will be a bias in the set of hits that the attenuation fit sees, and leads it to overestimate the light-level, and so under-estimate real hit energies by tens of percent. The approach adopted to solve this problem was to create a correction factor as a function of view, cell, and position along the cell which would be applied before the attenuation correction to remove the effect of thresholds and shielding. To this end MC truth information about the calibration hit sample is used to create a combined threshold and shadowing correction for each cell and view combination,

$$T = \frac{PE}{\lambda} \frac{E_{true}}{E_{mip}}, \quad (1)$$

where T is the combined “threshold and shielding” correction factor, PE is the simulated photoelectrons recorded at the readout, λ is the number of simulated photons which would be seen at the readout out in the absence of fluctuations, E_{true} is the true energy deposited in the cell and E_{mip} is the naive energy you would expect to be deposited based on the pathlength through the

312 cell. In this way it encodes a threshold correction based on the simulated readout PE with and
313 without the fluctuations, with λ dependent on your simulated threshold, as well as a shielding
314 correction based on the simulated energy deposition and a naive no shielding approximation.
315 This equation gives us a cell by cell correction but we use an empirical polynomial fit to that
316 distribution which removes statistical noise from the correction and well describes the initial
317 distribution. This correction factor is applied to the cell by cell data and MC PE/cm distributions
318 before the attenuation fits. [docdb:13579 - SA The Attenuation and Threshold Calibration
319 of the NOvA detector, reference 8 is for docdb:7247, a talk by Backhouse]

320 In the Far Detector, a large divergence between calibrated and true energies as a function of
321 W was observed. This was traced back to the much longer cell lengths in the FD meaning that
322 thresholds play a large role at the foot of a cell. For a hit to be seen above threshold there, it
323 may need to be a slight upwards fluctuation. This biases the set of hits that the attenuation fit
324 sees, and leads it to overestimate the light-level (and so under-estimate real hit energies) by tens
325 of percent. The approach adopted to solve this was to explicitly allow for this effect in the fits.
326 $W = 0$ was declared to have nominal amount of effect from thresholds, and corrections were
327 made to every other position to match that. In addition to writing histograms, CosmicCalib
328 now also writes TTrees, containing W , ADC, and pathlength. For a bin closer to the readout
329 than the centre, its energies are scaled down, and hits falling below threshold dropped, until its
330 median ADC/cm matches $W = 0$. This is then the value written into the profile, rather than the
331 actual median. For bins further away, it is hits at $W = 0$ that are dropped to determine the ratio.
332 These profiles are then fit in the usual way. This resolves the bulk of the problem in the FD. For
333 consistency, the same procedure should probably be applied in NDOS, although it is unlikely
334 to make much difference there. A remaining approx. 10% effect (Figure 5) is seen across the
335 Far Detector that is put down to self-shielding of cosmic rays by the detector mass. It behaves
336 as expected, monotonically in y , and symmetrically in x . I'd like to think of a scheme to allow
337 for this in some internal manner, rather than rely on a correction just taken straight from the
338 MC (otherwise why do we have a calibration procedure at all?), but it doesn't seem to be the
339 highest priority. [docdb:7410]

340 3.4 Relative calibration

341 Detailed description can be found in the "Instructions for the Attenuation Calibration Job"
342 technote from Prabhjot from docdb:13579 (list of all calibration technotes) and on the relative
343 calibration wiki page.

344 Relative calibration/attenuation correction (the exact commands are shown on figure 5).
345 This is taken from / inspired by Prabhjot technote. Maybe here I can just refer to the flowchart
346 for the commands but for TB I can specify what are the commands exactly. Maybe write down
347 a simple cook book for TB calibration.

- 348 1. Create the threshold/shadowing corrections
- 349 2. Create attenuation profiles, which are profile histograms of PE per pathlength as a func-
350 tion of w through each cell for all planes. The job is `makeattenuationprofileXjob.fcl`,
351 where X is `nndata`, `fddata`, `tbdta`, or `mc`. (For each individual cell create profile his-
352 tograms of average energy deposited per pathlength through the cell as a function of
353 position within a cell, i.e. PE/cm vs w .)

354 3. Analyse the calibhist files and draw the histograms

355 4. Do the attenuation fit using the attenuationfitjob.fcl

356 Create attenuation profiles Attenuation profiles have a constant binnin fNBins=100 (in
357 w), same for ND, FD and TB. This results in an effectively finer binning for TB compared
358 to ND and FD. For FD w = (-900,+900), ND: (-250,+250), TB: (-150,+150). TB: 3cm/bin,
359 ND: 5cm/bin, FD: 18cm/bin. What effect could this have on the relative calibration results?
360 Particularly on the calibration shape?

361 Do the fit. What exact fits are we using and in what order? Exponential, fit to residuals...

The attenuation fit considers both short- and long-path light (i.e. when a photon goes straight to the readout and when it loops around the cell first). The profile in a channel is fit to the form,

$$y = C + A \left(\exp\left(\frac{W}{X}\right) + \exp\left(-\frac{L+W}{X}\right) \right), \quad (2)$$

362 where y is the response, L is the cell length, C, A and X are the free parameters in the fit. X
363 gives the attenuation length as well. Initially, the fit is to the central part of the cell, which
364 is different for each detector. In addition to the approximately quartic behavior at the ends of
365 every channel there are in many channels fairly large residuals. They don't appear to follow
366 any consistent pattern. The leading hypothesis is that these are due to varying fiber position
367 within the cell. Usually the fiber lies in the corners of the cell, but if it is somehow twisted so
368 that it rises into the center of the cell, then it should collect more light, to an extent comparable
369 to what is seen here. To remove such an irregular pattern, the residual from the analytic fit
370 is simply fit with LOcally WEighted Scatter plot Smoothing, LOWESS. The LOWESS curve
371 at each point is formed from the weighted mean of the deviations. The weighting function is
372 the traditional tri-cube, (insert equation, likely not needed for this technote) [docdb:13579 -
373 SA The Attenuation and Threshold Calibration of the NOvA detector, already in 1stAna and
374 Backhouse's technote]

375 For NDOS the fit was a very little bit different, where we didn't use L but $3L/2$. Also it says
376 that "Over the length of an NDOS cell, the effect of the long attenuation length is imperceptible,
377 and is modelled as a constant (If you put a long attenuation term in, the fit drives the length
378 scale to infinity anyway). [docdb:7410]

In many channels, fairly large residuals are visible. They don't appear to follow any consistent pattern. The hypothesis is that these are due to varying fibre position within the cell. Usually the fibre lies in the corners of the cell, but if it is somehow twisted so that it rises into the centre of the cell, then it should collect more light, to an extent comparable to what is seen here. To remove such an irregular pattern, the residual from the analytic fit is simply fit with LOWESS (locally weighted scatterplot smoothing). The LOWESS curve at each point is formed from the weighted mean of the deviations. The weighting function is the traditional tri-cube:

$$w_i = \left(1 - \left| \frac{x - x_i}{\sigma} \right|^3 \right)^3. \quad (3)$$

379 The smoothing length scale σ is 30cm. 20 points calculated by this method are stored, to be
380 linearly interpolated between to approximate the full LOWESS curve. If the LOWESS fit at
381 any point exceeds 15% the original attenuation fit was very bad, and the channel is marked
382 uncalibrated. Figure 4 shows an example of large (10%) deviations being fitted. This variation

383 is not seen in the MC, and so the LOWESS fit is skipped there. Due to the lower stats available
384 in MC, instead of being collated by plane and cell, the curves are only calculated by view and
385 cell. [docdb:7410]

386 The current value of σ in the code is $1.5 \times \text{DetWidth}/20$

387 Now we have the relative calibration done and the constants saves. What are the const and
388 points files that we get? What do they mean?

389 3.5 Absolute calibration

390 Apply cuts and get an average PEcorr response for each epoch/period individually and for each
391 view. Get an average over the two views.

392 Save the results.

393 Stopping muons provide a good sample of known energy deposits. If we can collect a
394 “golden” sample, they should provide the scale factor to convert PEcorr to GeV. So far, the
395 method used has been imperfect, and the absolute calibration constants are known to be off
396 by approx. 10%. Since a factor already has to be derived to correct for dead material, this is
397 not significantly impeding current efforts, but work was recently gone into improving this area.
398 [docdb:7410 - this was likely before the track window cut was introduced] (Here it says that it's
399 not such a big a problem since we have to scale for the dead material anyway. But nowadays we
400 have to account for a large systematic uncertainty in the absolute energy scale in our analyses.
401 How is the dead material correction different from the energy scale uncertainty?)

...the calibration of the calorimetric energy scale of the NOvA detectors uses the energy deposited by stopping muons as a standard candle. To reduce systematic uncertainties, only those energy deposits in a 1-2 m window away from the muon track end point are used. The mean of the detector response distribution is found for data and MC in both near and far detectors. The mean of the distribution of true energy deposits in the track window is used to provide a conversion factor between the detector response and the true energy deposited in the scintillator for minimum ionising muons. The simulated dE/dx is uniform within about 1.8% for hits around the minimum between 100-200 cm from the track end. The energy that a muon deposits within each cell is estimated using Geant 4 and stored in Fibre Liquid Scintillator (FLS) hits. FLS hits are only those within the active material (liquid scintillator) and energy loss within the passive material (plastic extrusions) is ignored. an estimate of the minimum energy loss rate of stopping muons in the NOvA scintillator is found to be,

$$\left. \frac{dE}{dx} \right|_{\text{mip}} = (1.7915 \pm 0.0035) \text{ MeV/cm.} \quad (4)$$

402 For stopping muons in NOvA it is also important to consider their decay. The muon has a vacuum lifetime of about 2.2 microseconds and favourably decays, with a branching ratio approx.
403 100%, into an electron, an electron anti-neutrino and a muon neutrino. The electron produced
404 in this decay is called a Michel electron and is used to select muons that stop within the NOvA
405 detectors. The energy scale calibration is performed using cosmic ray muons. The calibration
406 measures the detector response in data and MC in both near and far detectors and normalises
407 them all by providing a conversion factor, for all four cases, that converts the detector response
408 to energy in GeV. The energy loss rate (dE/dx) of stopping muons is well described by the
409 Bethe-Bloch and is a function of the distance from the stopping point. A track window technique
410 is used to minimise the variations in detector response that depend on the distance to

412 the track end. Using this technique only hits within a region of distances from the track end
413 are used. The position of the track window is chosen such that a mis-reconstruction of the
414 track end point has the minimum effect on the mean detector response. The track window is
415 currently set to be in the range from 100 cm to 200 cm from the track end.[docdb:13579 -
416 FA_Calorimetric_energy_scale]

417 In the First Analysis An adjustment was made to the value for the ND data to lower the
418 value of PEcorr/cm by about 3.6%. The adjustment was made based on studies of muons from
419 beam neutrinos interacting in the detector where it was observed that the average beam muon
420 response was 3.6% lower in data than in MC [8]. For the FD There is a discrepancy in the
421 distributions of PEcorr/cm in data and MC; the mean of the distribution is higher in data than
422 in MC. This may be due to mis-modelling of the detector response in the MC. In any case, the
423 data-MC PEcorr/cm discrepancy is tuned out when the calorimetric energy scale is applied.
424 [docdb:13579 - FA_Calorimetric_energy_scale]

425 The calibration constants are written to the database tables calib atten consts and calib atten
426 points. The calib atten consts table contains the seven free parameters in the attenuation fit, plus
427 identifying information. The calib atten points table contains the 20 LOWESS points for each
428 cell, with one point per row. When a request comes to Calibrator to create a RecoHit, usually
429 from a RecoBase object that has provided a W value based on a straight-line extrapolation of its
430 trajectory, ultimately we end up in Calibrator::GetPEcorr. This retrieves an AttenCurve object
431 from a cache we hold of all the database values, which can calculate the mean response to
432 cosmic rays at any position. The calibrated energy deposit is then the PE in the CellHit divided
433 by this average cosmic ray response. A correction factor taken from the absolute calibration,
434 also stored in the database, is applied to the answer to give the resulting PEcorr. Calibrator also
435 stores the quality of the calibration fit for a given cell such that if we fail to calibrate a cell in the
436 Data to a sufficient quality that cell will not return a calibrated energy in both Data and Monte
437 Carlo. Calibrator also returns the MIP and GeV scales that are described in the accompanying
438 absolute calibration technote. [docdb:13579 - SA The Attenuation and Threshold Calibration
439 of the NOvA detector] ...The calibrated energy deposit is then the PE in the CellHit divided
440 by this average cosmic ray responseAn eyeballed factor of 75 is applied to the answer to give
441 the resulting PEcorr about the same size as the input PE (this is the factor (originally) used)
442 [docdb:7410]

443 3.6 Calibration uncertainties

444 First Analysis systematic uncertainties due to calibration: Sources of systematic uncertainty
445 of particular concern are those introduced by residual variations remaining after calibration.
446 Systematic errors are introduced by spatial and temporal variations in detector response. Fur-
447 ther, any difference between the two detectors may introduce a relative shift in the energy
448 scale between the detectors. A source of systematic uncertainty can be introduced by mis-
449 reconstructing the end point of the muon track. Such a mis-reconstruction would shift the
450 window within which hits are selected and hence the dE/dx of the muon. The figure shows
451 that the detector response varies by up to about 60% over the range from 0 to 500 cm to the
452 track end. This large variation illustrates the importance of careful consideration of the track
453 window position and size. The detector response for both data and MC is minimum at about
454 130 cm from the track end and is flat to about 1% in the range from 100 cm to 200 cm from
455 the track end. For a track window starting at 100 cm from the track end, a conservative mis-

reconstruction of the track end point by 10cm will shift the start of the track window to between 90cm and 110cm. This shift will alter the MEU value by less than 0.4% over the range. If the calibration procedure was ideal the detector response would not vary with position in either data or MC. The calibration is not ideal and the detector response and recorded simulated energy deposition varies with position of the hit within the detector, such variations will introduce systematic errors. The position of a hit can be defined by the plane, cell within the plane, and distance along the cell (w) of the hit. The variation in detector response and simulated energy deposition vs. plane, cell and w for each view has been studied to quantify the systematic uncertainty introduced by these sources. The rise in detector response at the far end of FD y-view cells is an issue with several potential sources. The rise in response may be due to an acceptance effect or a light-level threshold effect among other possibilities. An acceptance effect is where greater energy must be deposited at the far end of the cells so that the light can travel along the fibre, hit the APD and be recorded as a hit. Both an acceptance effect and a light-level effect would introduce a bias towards higher energy hits toward the far end of cells. Another source of systematic uncertainty is introduced by the variation in detector response with time. The FD response is stable to about 1% during the period from October 2014 to March 2015. The ND response needs further study but there was no significant trend over 6 months at 5%. As mentioned in Section 5, the version (7.1) of the calibration used for first analysis has been adjusted based on studies of muons from beam neutrinos interacting in the detector [8]. A shift of 3.6% was introduced based on the average response of muons where large sections of the track were used. When only a track window of 100-200cm is used on the beam muons the difference is only 2.7% [8]. Our best hypothesis for this residual 2.7% difference is that it is caused by showery events that are present in ND data but not ND MC: it was shown in [9] that doing the calorimetric energy scale calibration using a truncated mean (or a median or a fit to the peak) gave a data/MC ratio that differed by 2.7% compared to using the untruncated mean as described in this document. A comparison of various cross checks of the calorimetric energy scale was undertaken (in [10] and [11]) and concluded that the nearly 5% difference between ND data and MC seen in a sample of Michele electrons [12] should be applied as both an absolute and relative shift to the calorimetric energy scale. The difference between the level of calorimetric energy resolution of stopping muons was studied and it was found that data and MC agreed best when an 8% additional smearing was introduced. Studies for the NuMu analysis indicated that this was a negligible systematic uncertainty [13]. [docdb:13579 - FA_Calorimetric_energy_scale]

4 NOvA Test Beam detector calibration

4.1 Overview

History of TB calibration. What led to the final version of TB calibration. What can be done next.

Dates and times when the data taking occurred.

From Calibration_Meta_READFIRST.pdf: Validations of any calibration correction take the same basic form:

1. What deficiency are you correcting for? (For Test Beam this would be the difference between the different scintillators, also the faulty FEBs, distribution of w is not flat,

especially in the overfilled cells. The energy response between the different cells and planes is not the same. Maybe I should talk about this for each period separately when I have the calibhist plots which show the non-linearities. Also the PhotonTransport plots don't really show the PECorr but the PE/cm itself but with the fit!!!

2. What correction factors/scales have you found? Show them in plot form. (This is basically the PhotonTransport plots for the relative calibration and the pecorrcm distributions for the absolute calibration)
3. Now generate the same plots as in (1) but with the corrections applied. Technically this is the absolute calibration validation plots. Does this mean that the PE/cm plots from the absolute calibration should be/are exactly the same as the calibhist plots? Not entirely as those are only for the stopping muons, whereas the calibhist are for the through-going muons. Does it mean I should maybe generate the calibhist plots with the relative calibration applied?
4. Ratios of plots in (3) to (1) to highlight any patterns or difficult-to-spot discrepancies between what we think should happen when the constants are applied, and what does happen. But what does this tell us? It's basically just an average of the attenuation correction...

Period naming, possibly epochs (for P3). List of data samples, plus MC samples that were used and pointer to the data-based simulation technote.

Specific running conditions: - maybe enough to mention this in the individual descriptions of the test beam periods Underfilled cells Faulty FEBs (Period 2 and Period 3)

Why do we do the calibration generally and why do we need to do in for Test Beam specifically - probably in the introduction

Temperature study (small overview)

From Teresa's thesis Along with setting the energy scale of the detector, we need to calibrate the timing of the readout system for the detector. The Data Concentrator Modules (DCMs) responsible for collating the data from multiple FEBs get their timing information via a daisy chain originating at the detector TDU. Each DCM in the chain has a timing offset relative to the DCM before it, with the last DCM having the earliest ti. Following the procedure described in [66], I used timing information from hits on cosmic ray muon tracks that pass through multiple DCMs to determine the relative offsets between DCMs, shown in Figure 3.20.

4.1.1 Definitions

List all final data and simulation definitions used.

From Teresa's thesis: "For Test Beam, we have three beam-based triggers, one pulsed trigger, and two data-driven triggers. The data-driven triggers are both activity-based triggers. The first is intended to record cosmic ray induced events for use in calibrating the detector."

4.2 Detector Brightness

4.3 Threshold and shielding corrections

The threshold and shielding correction for test beam is almost uniform across all cells as can be seen on figure... This is expected as the hight of the Test Beam detector of 2.6m has only a

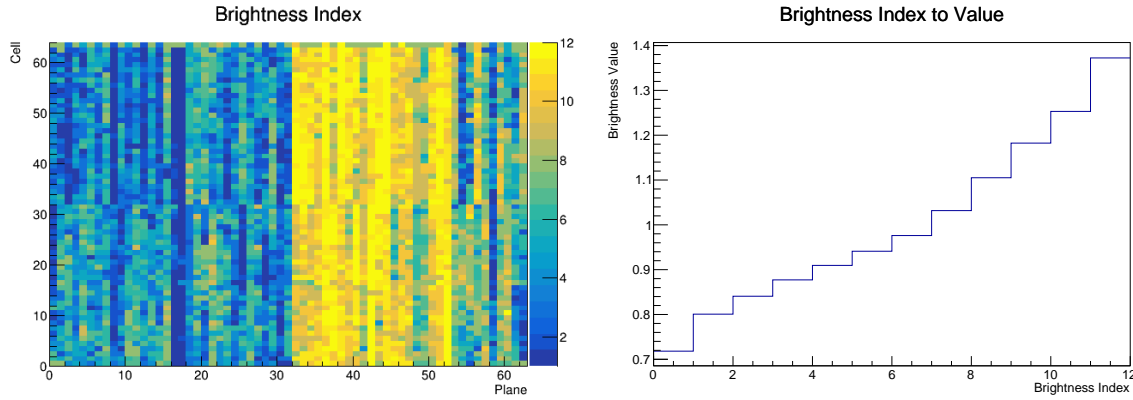


Figure 6: The Test Beam detector is (like the standard NOvA detectors) divided into 12 brightness bins (left plot), each representing a relative difference in energy response (right plot) due to different brightnesses of the fibers, scintillators, or readout.

negligible effect on the energy distribution of cosmic muons or on the threshold saturation. The correction is basically just a normalization factor, but since the relative calibration only cares about relative differences across the detector, a normalization factor doesn't change anything.

4.4 Simulation

We originally used Teresa's calibration MC sample, but after we saw disagreement, we developed a new MC based off of the period 3 data, which we ended up using for both period 2 and period 3. For fibre brightness we are also using the same MC from period 3 data as it represents the detector in its best condition.

We used a data-based simulation of cosmic muons for the Test Beam detector calibration. The details are described in the technote XXX. We used this and this data as a basis and this and this data for the fiber brightness file.

4.4.1 Relative calibration results

4.5 Period 1

Only a month of data, only first half of detector filled, primary/secondary beam halo, or oversaturation leading to FEB shutoffs [docdb:38349 and 41331]. Only used for commissioning, not used for any data analysis or calibration.

4.6 Period 2

What was done for the period 2 tb calibration, short overview of what has been done: test beam data were calibrated all at the same time without splitting them to separate epochs. See figures 11, 12 and 13.

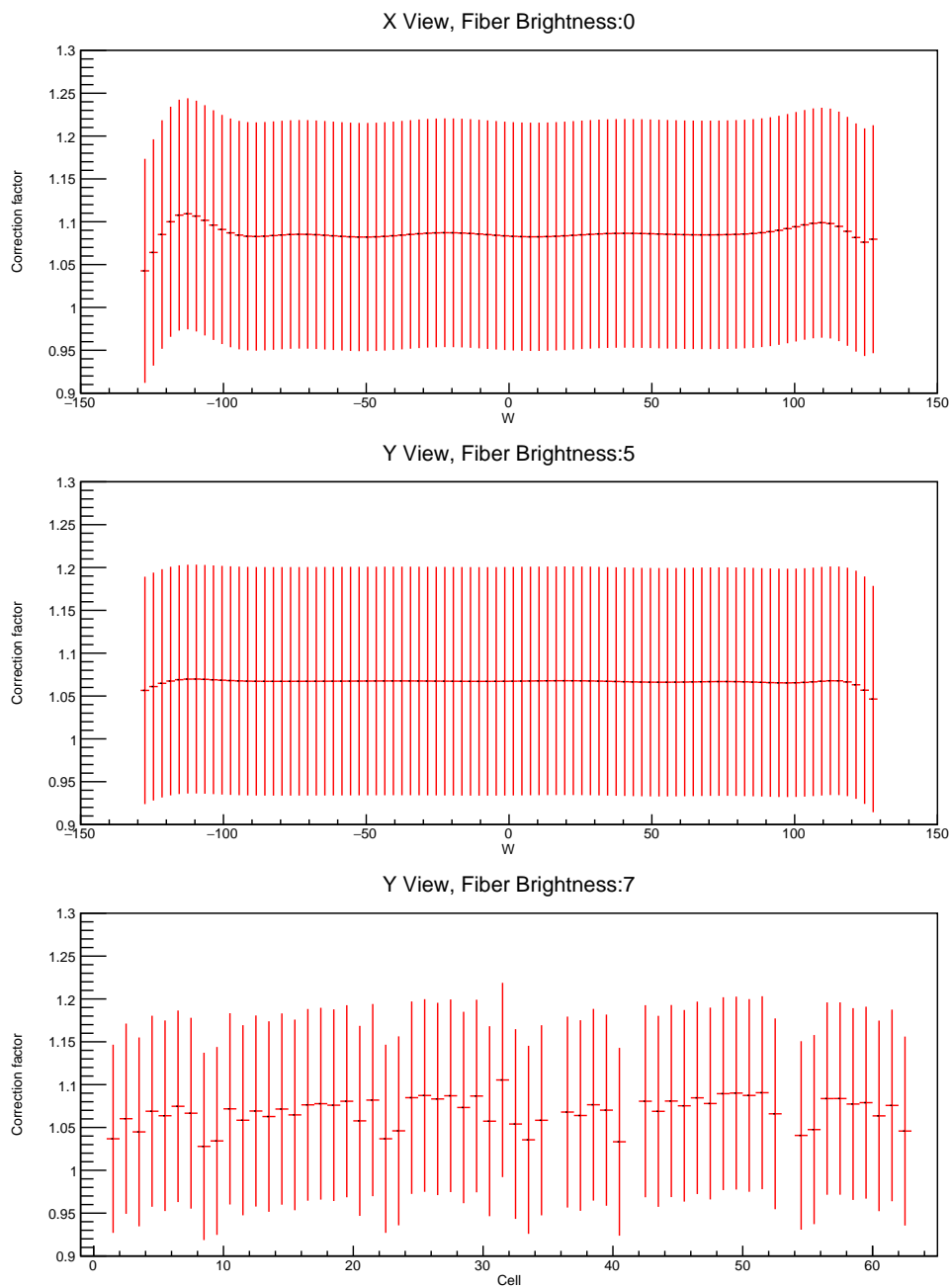


Figure 7: Examples of threshold and shielding corrections for the Test Beam detector

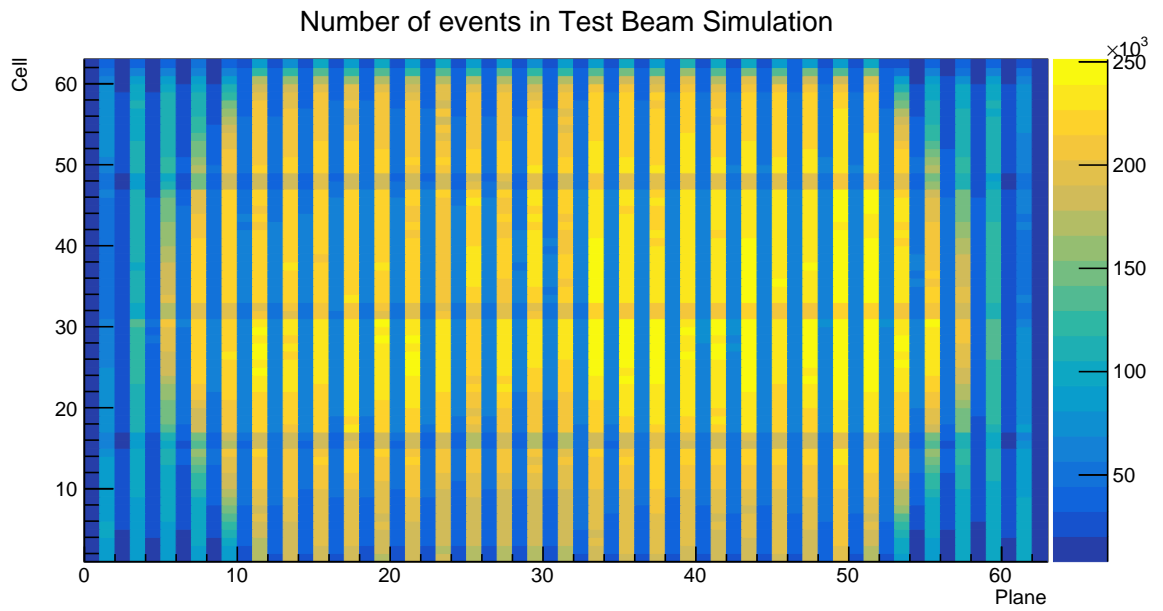


Figure 8: Distribution of events in the Test Beam simulation calibration sample.

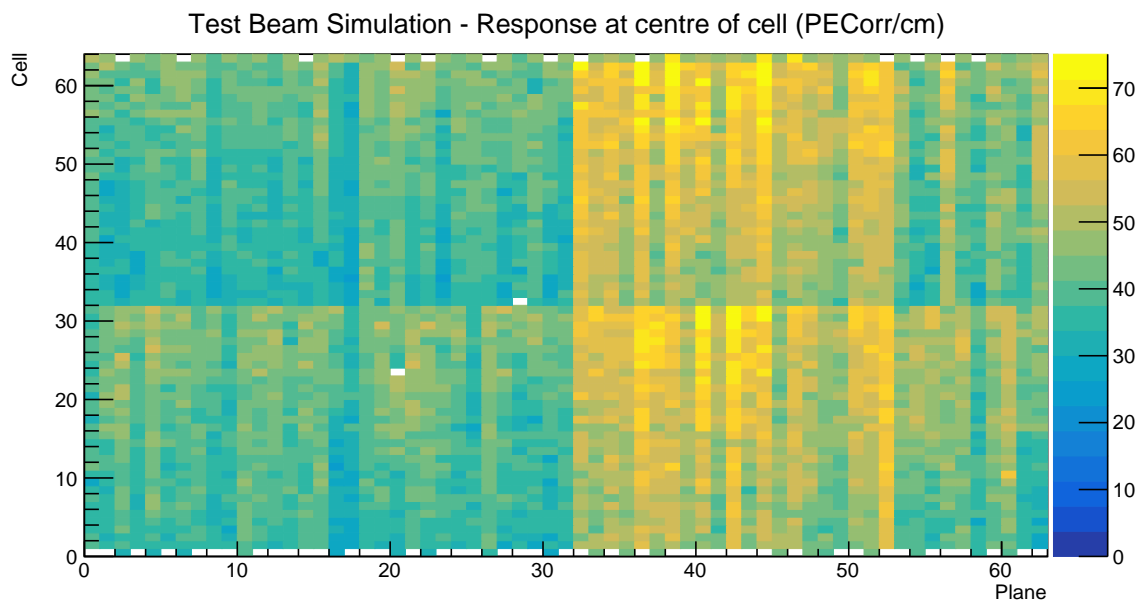


Figure 9: Overview of the relative calibration results for the Teast Beam detector simulation. Each cell is represents the average corrected energy response (in PECorr/cm) in the centre of each cell. The blank cells are uncalibrated.

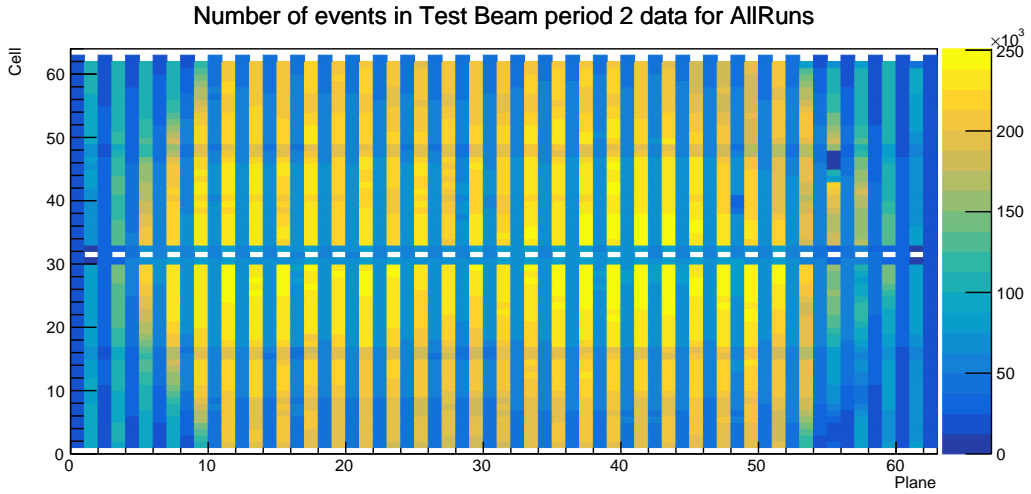


Figure 10: Distribution of events in the period 2 Test Beam data calibration sample.

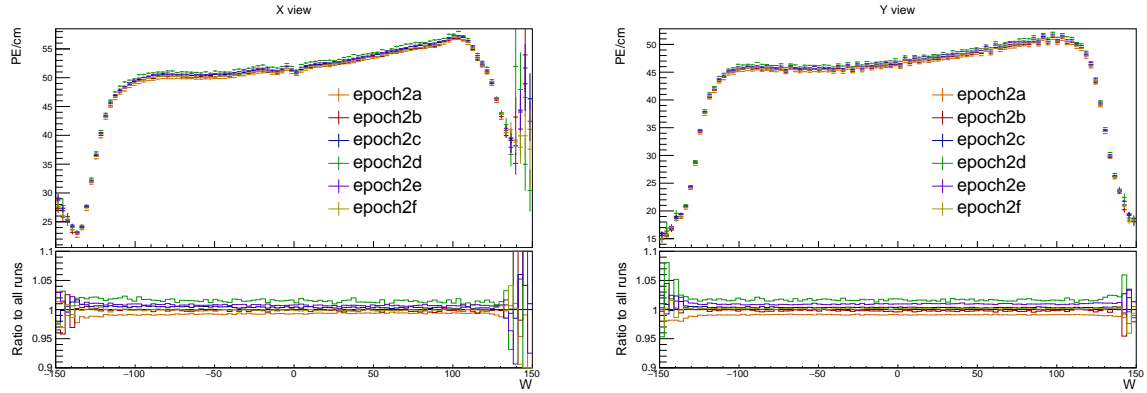


Figure 11: Uncorrected average energy response as a function of the position within a cell (w) for epochs in period 2. It is clear that there is no significant difference between the various epochs.

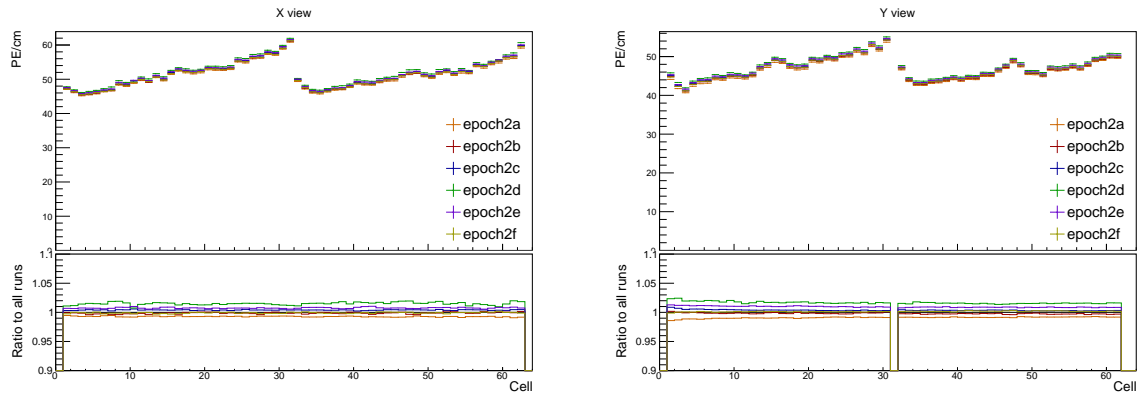


Figure 12: Uncorrected average energy response as a function of cells for epochs in period 2.

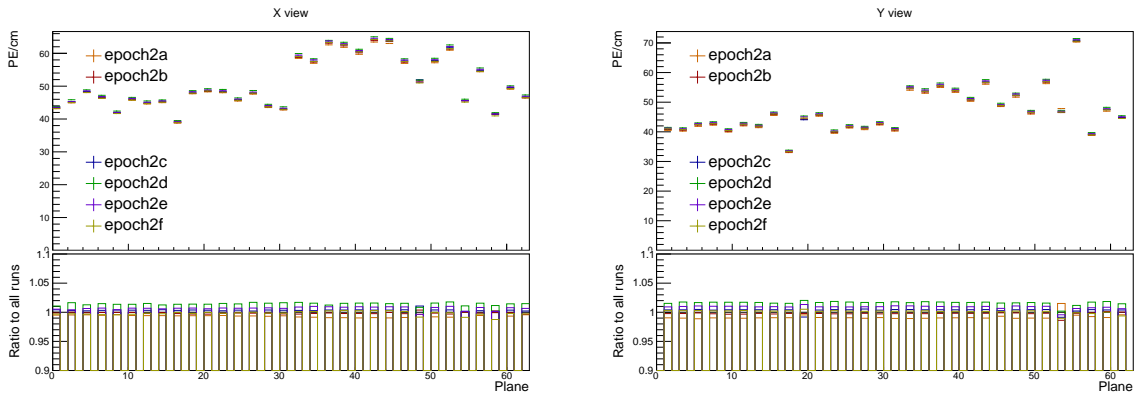


Figure 13: Uncorrected average energy response as a function of planes for epochs in period 2.

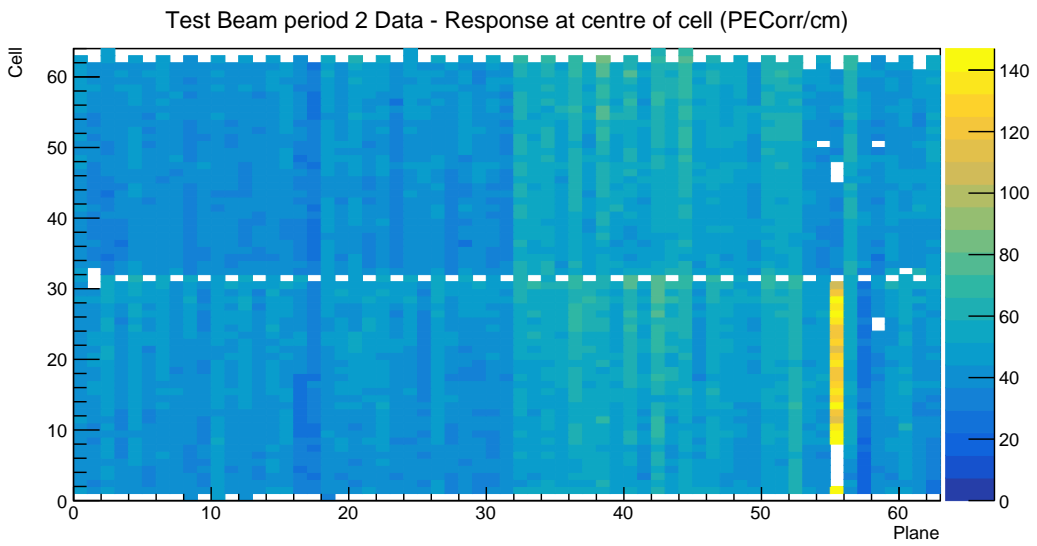


Figure 14: Overview of the relative calibration results for the Teast Beam detector period 2 data. Each cell is represents the average corrected energy response (in PECorr/cm) in the centre of each cell. The blank cells are uncalibrated.

558 **4.6.1 Relative calibration results**

559 **4.7 Period 3**

560 Separation of Period 3 data into different epochs based on the running conditions (include plot
561 of the running conditions). We are separating data into pre- and post- filling states. We're using
562 only the fully-refilled post-FEB swap data from period 3 as a basis for the simulation creation.

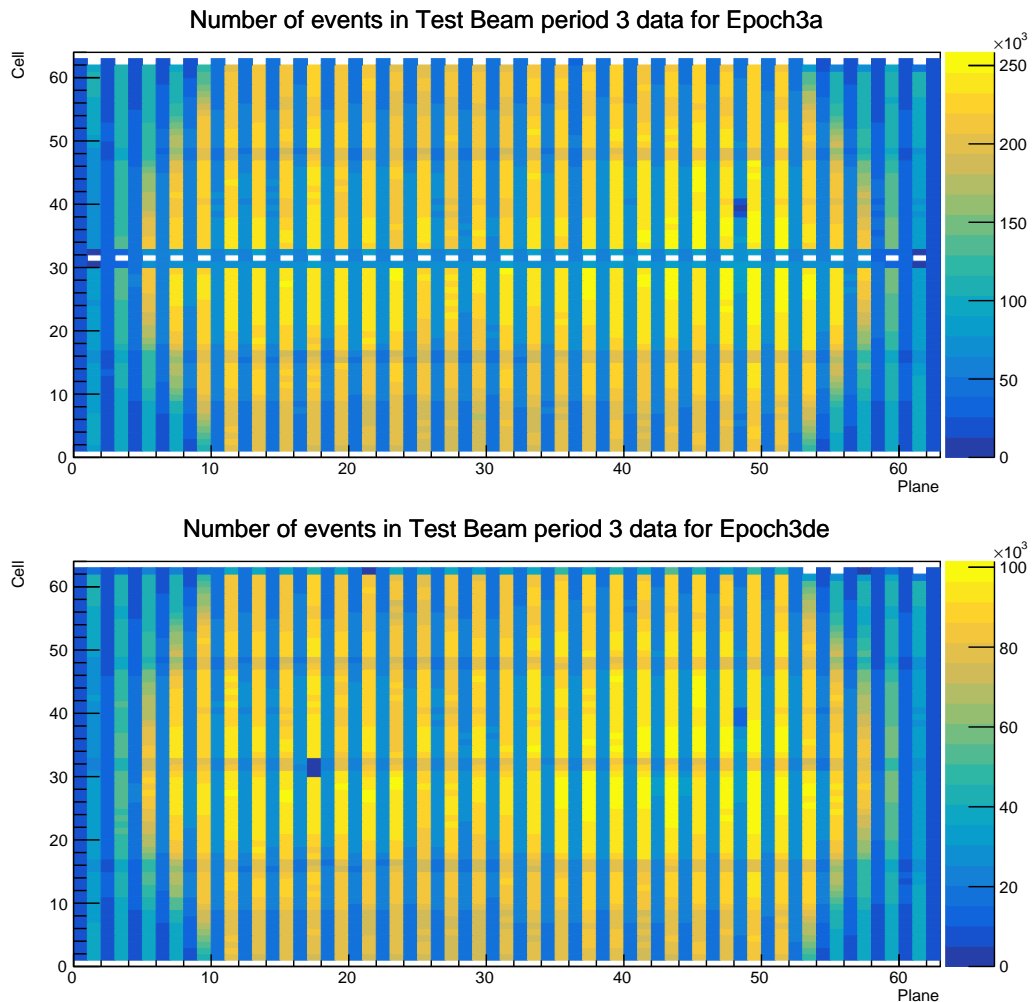


Figure 15: Distribution of events in the period 3, epoch 3a Test Beam data calibration sample.

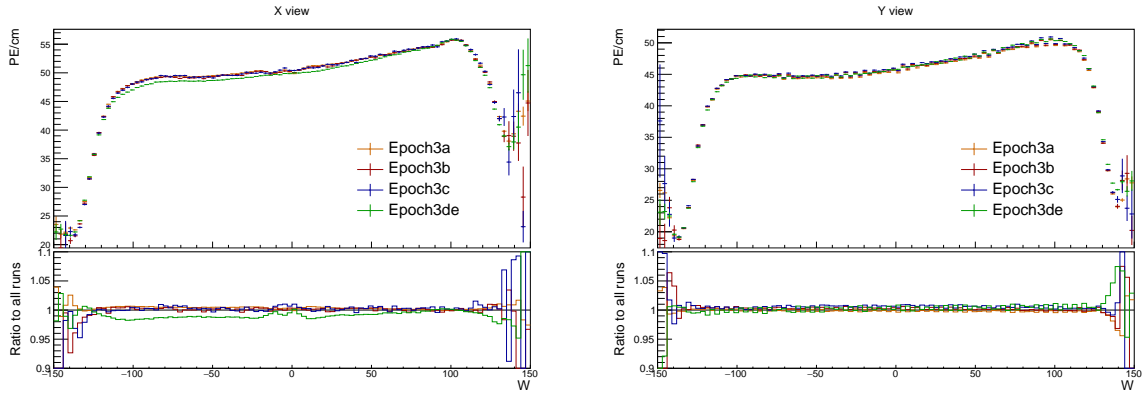


Figure 16: Uncorrected average energy response as a function of the position within a cell (w) for epochs in period 3.

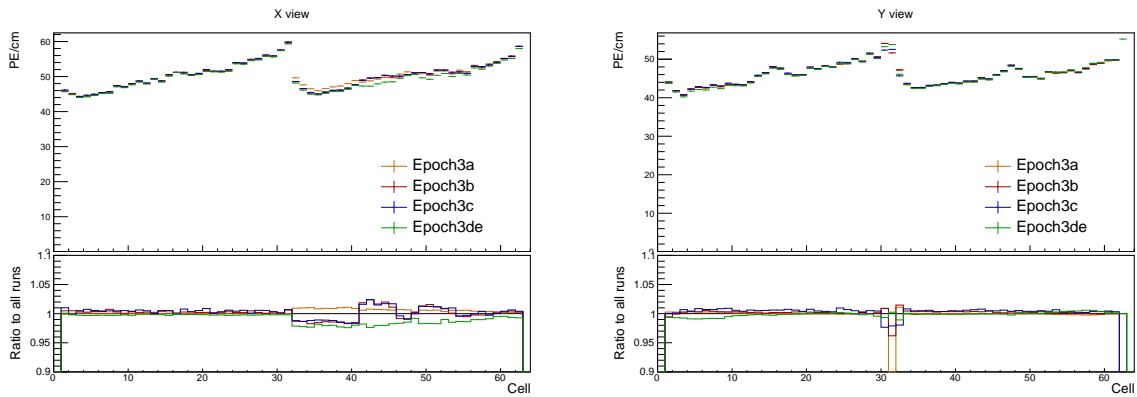


Figure 17: Uncorrected average energy response as a function of cells for epochs in period 3.

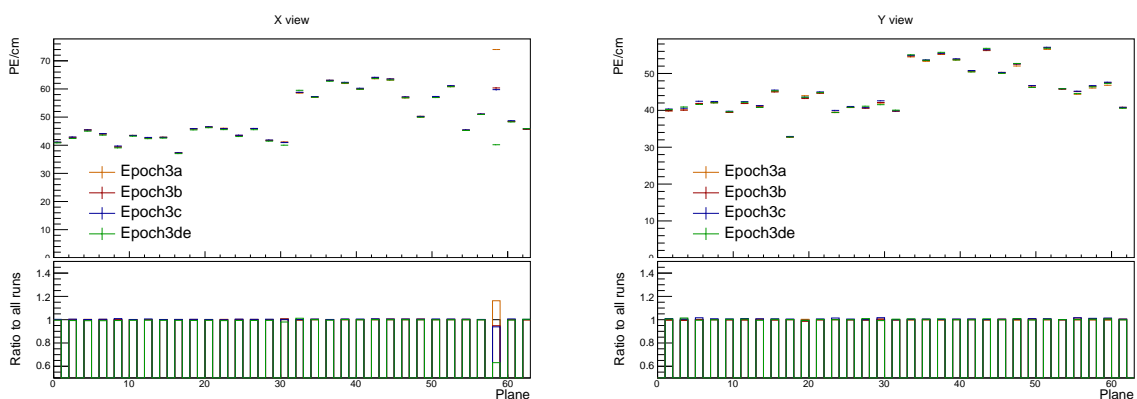


Figure 18: Uncorrected average energy response as a function of planes for epochs in period 3.

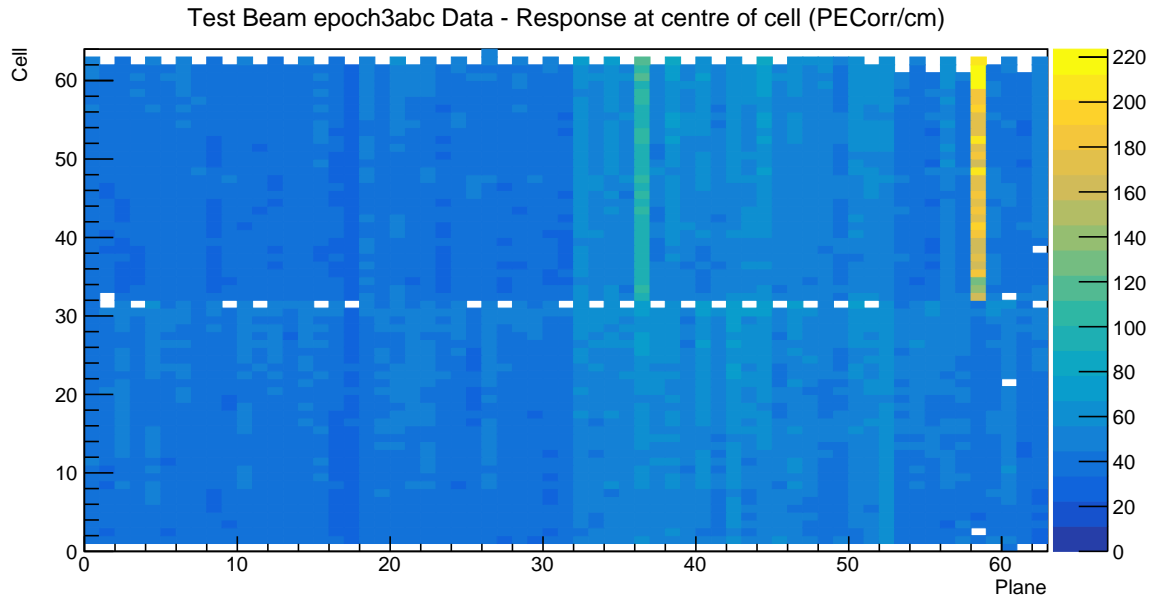


Figure 19: Overview of the relative calibration results for the Teast Beam detector period 3, combined epochs 3a, 3b and 3c data. Each cell is represents the average corrected energy response (in PECorr/cm) in the centre of each cell. The blank cells are uncalibrated.

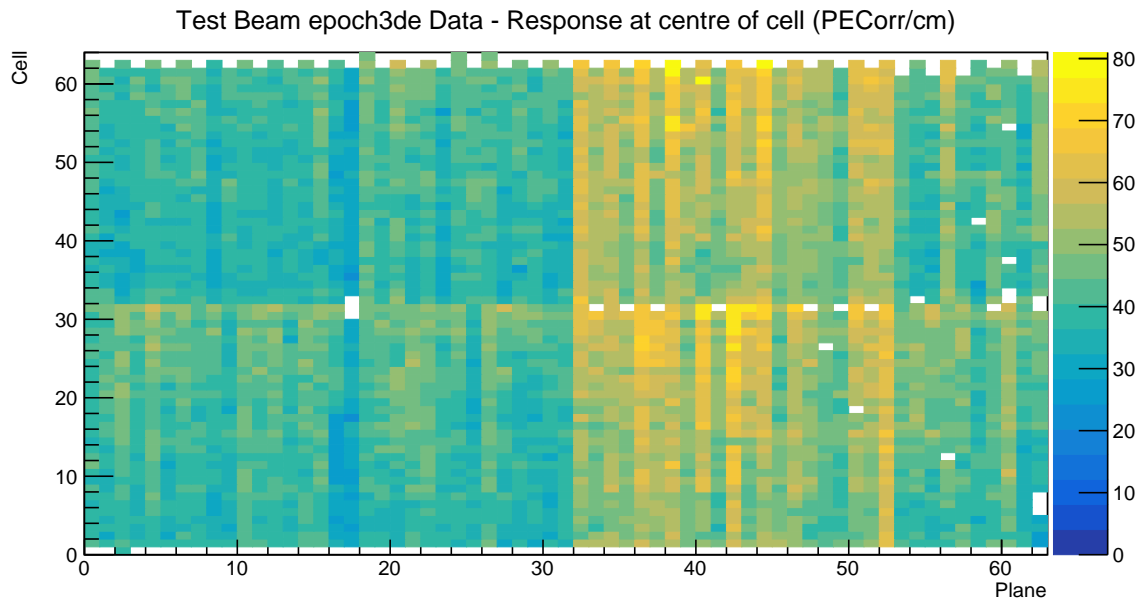


Figure 20: Overview of the relative calibration results for the Teast Beam detector period 3, combined epochs 3d and 3e data. Each cell is represents the average corrected energy response (in PECorr/cm) in the centre of each cell. The blank cells are uncalibrated.

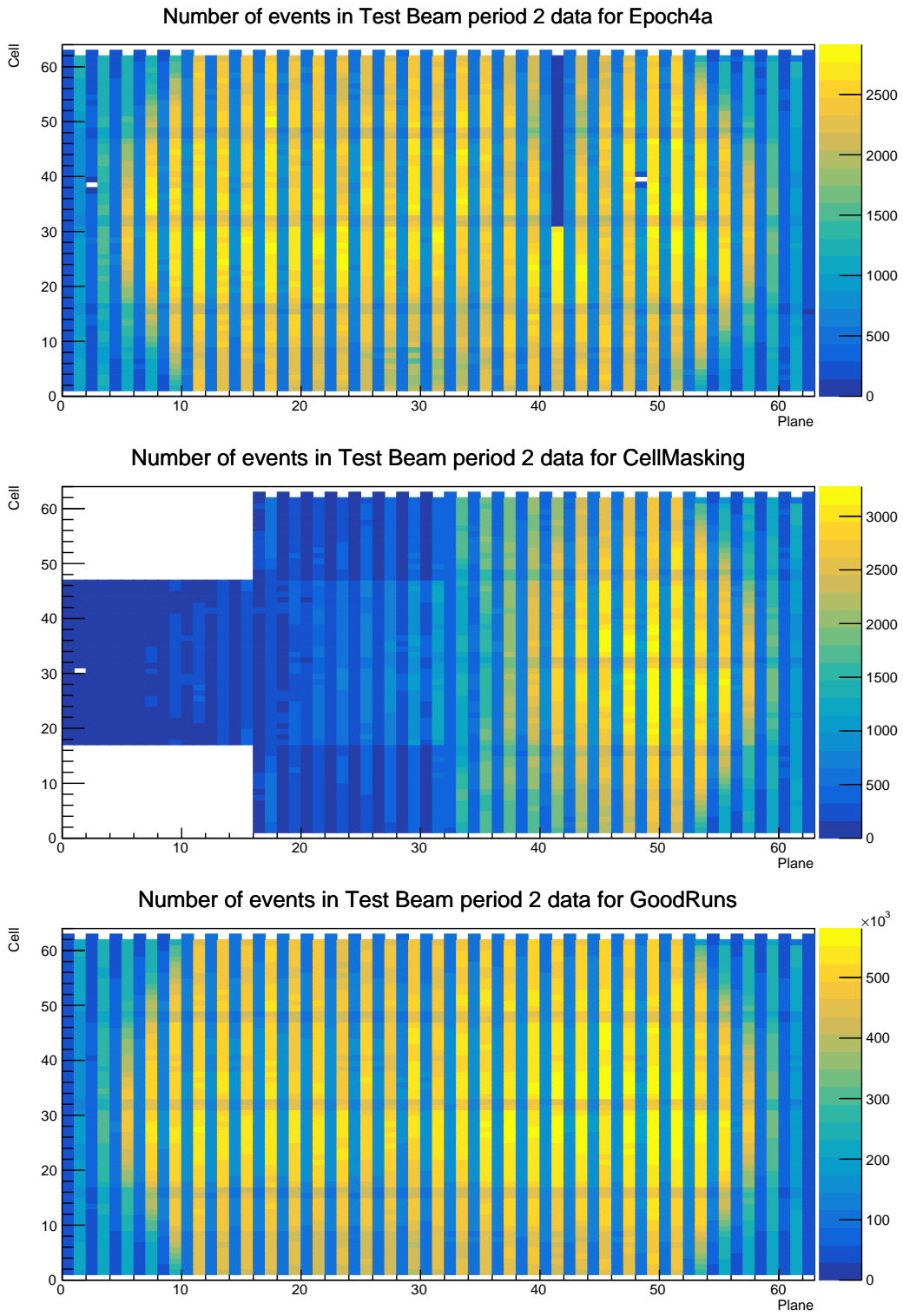


Figure 21: Distribution of events in the Test Beam period 4 data calibration sample. The top plot shows the first three commissioning runs, the middle plot the status of the detector during the Cell Masking studies and the bottom plot shows the rest.

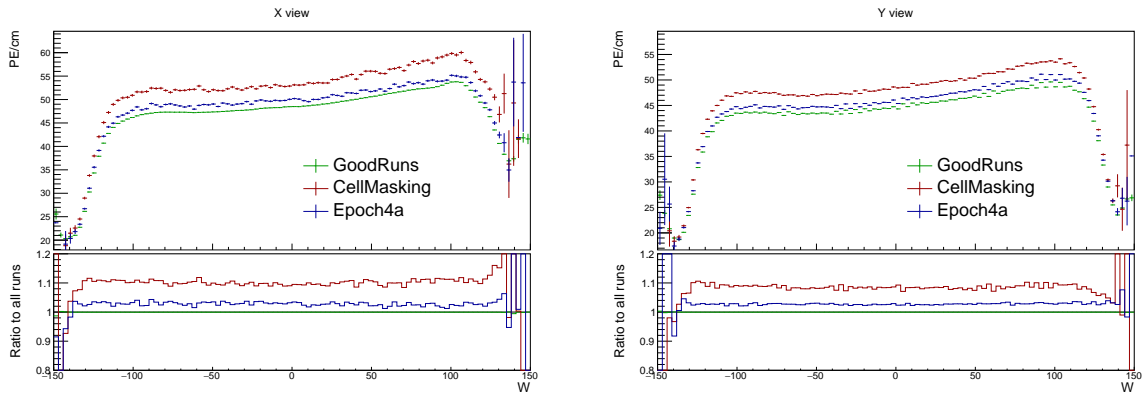


Figure 22: Uncorrected average energy response as a function of the position within a cell (w) for epochs in period 4.

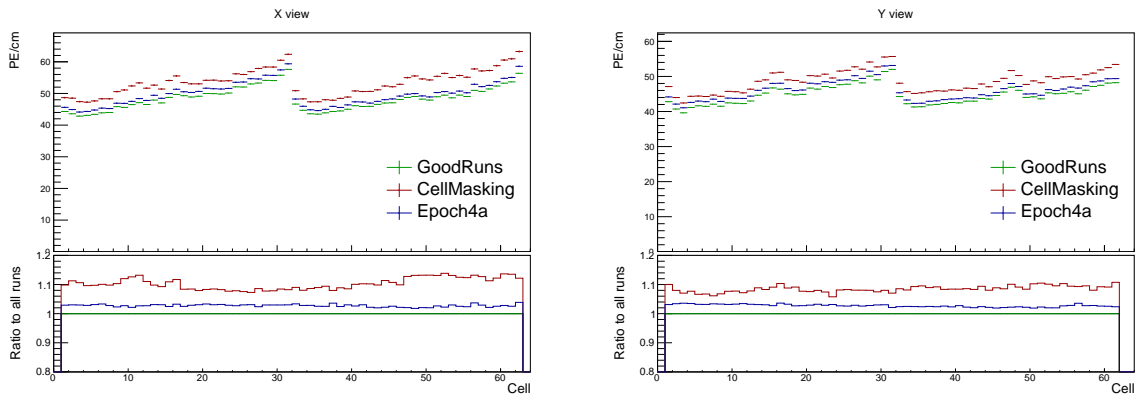


Figure 23: Uncorrected average energy response as a function of cells for epochs in period 4.

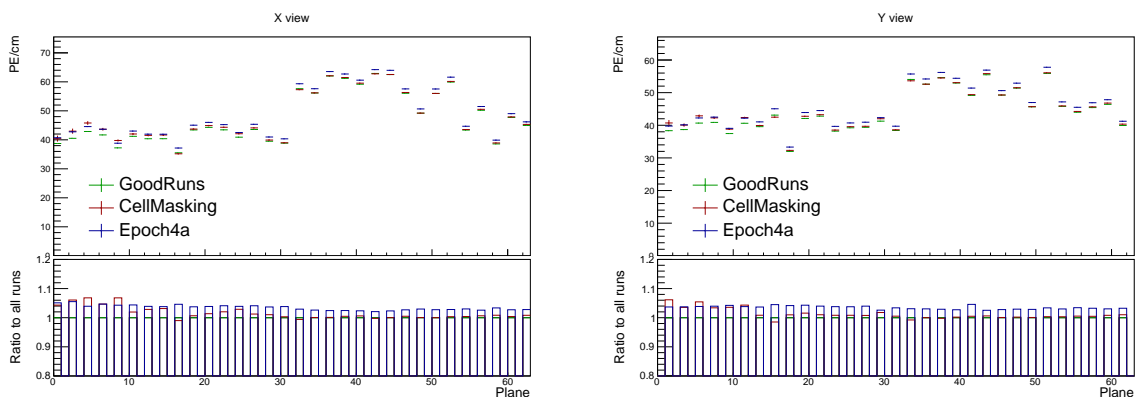


Figure 24: Uncorrected average energy response as a function of planes for epochs in period 4.

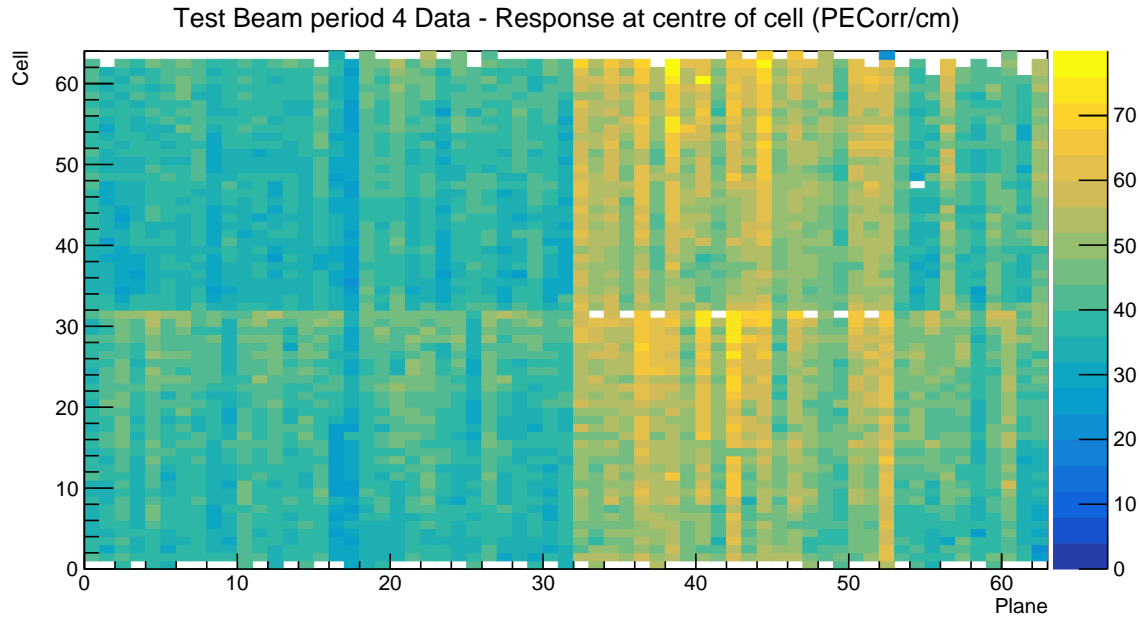


Figure 25: Overview of the relative calibration results for the Teast Beam detector period 4 data. Each cell is represents the average corrected energy response (in PECorr/cm) in the centre of each cell. The blank cells are uncalibrated.

⁵⁶³ **4.7.1 Relative calibration results**

⁵⁶⁴ **Combined epochs 3a, 3b and 3c**

⁵⁶⁵ **Combined epochs 3d and 3e**

⁵⁶⁶ **4.8 Period 4**

⁵⁶⁷ **4.8.1 Relative calibration results**

⁵⁶⁸ **4.9 Absolute calibration results**

⁵⁶⁹ Standard absolute calibration cuts: track window, flat-response W, positive pe, pecorr, and
⁵⁷⁰ pathlenght reco

Sample	NHitsx	MEUx	NHitsy	MEUy	MEU	MEU Err	TrueE/dx	tE/dx Err
epoch 3abc data	2.638e+05	38.49	1.621e+06	39.4	38.94	0.006758	1.772	0.000238
epoch 3de data	1.049e+05	38.63	6.725e+05	39.42	39.02	0.01048	1.772	0.000238
period 2 data	2.322e+05	38.7	1.413e+06	39.4	39.05	0.007252	1.772	0.000238
period 4 data	5.268e+05	38.63	3.316e+06	39.4	39.01	0.004703	1.772	0.000238
simulation	2.829e+05	40.17	1.842e+06	39.93	40.05	0.006418	1.772	0.000238

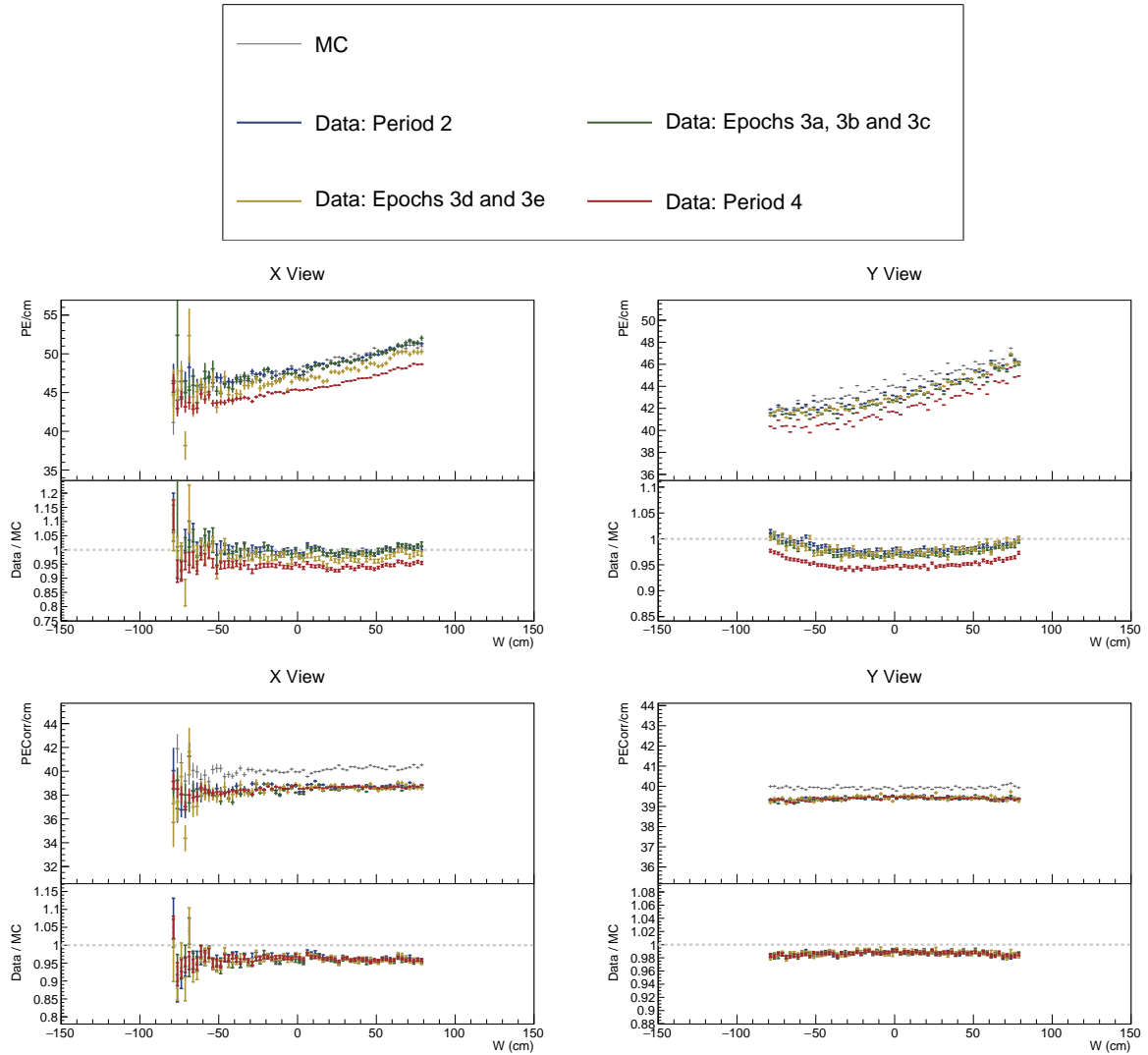


Figure 26: ...

572 4.10 Drift in TB data

573 4.11 Results

574 Table of final results. Final CSVs are located in the /nova/ana/testbeam/calibration and
 575 they have been included in the vXX.XX calibration tag.

576 Plots of absolute calibration results

577 4.12 Validation

578 Comparisons with older version of calibration and maybe with the FD and ND

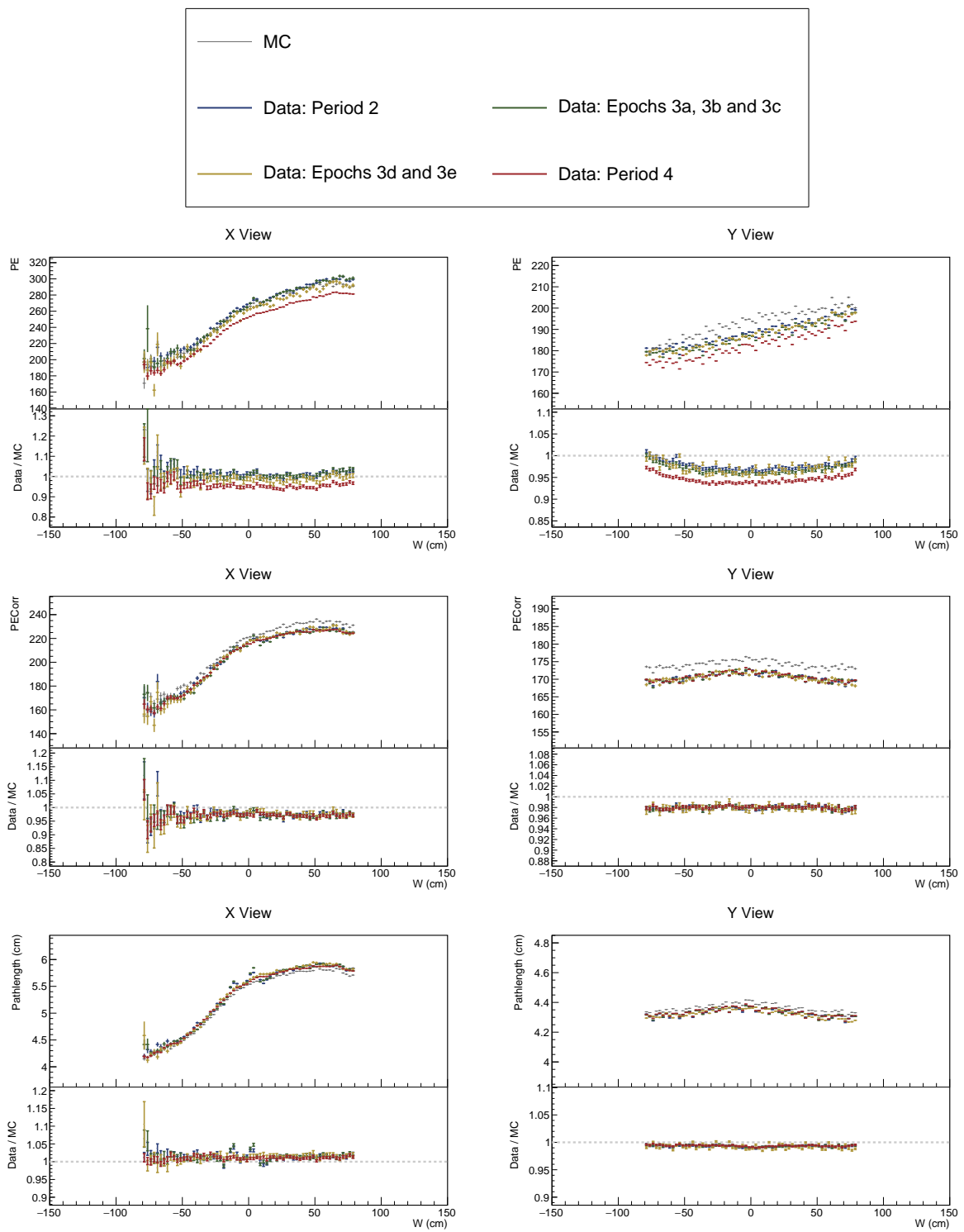


Figure 27: ...

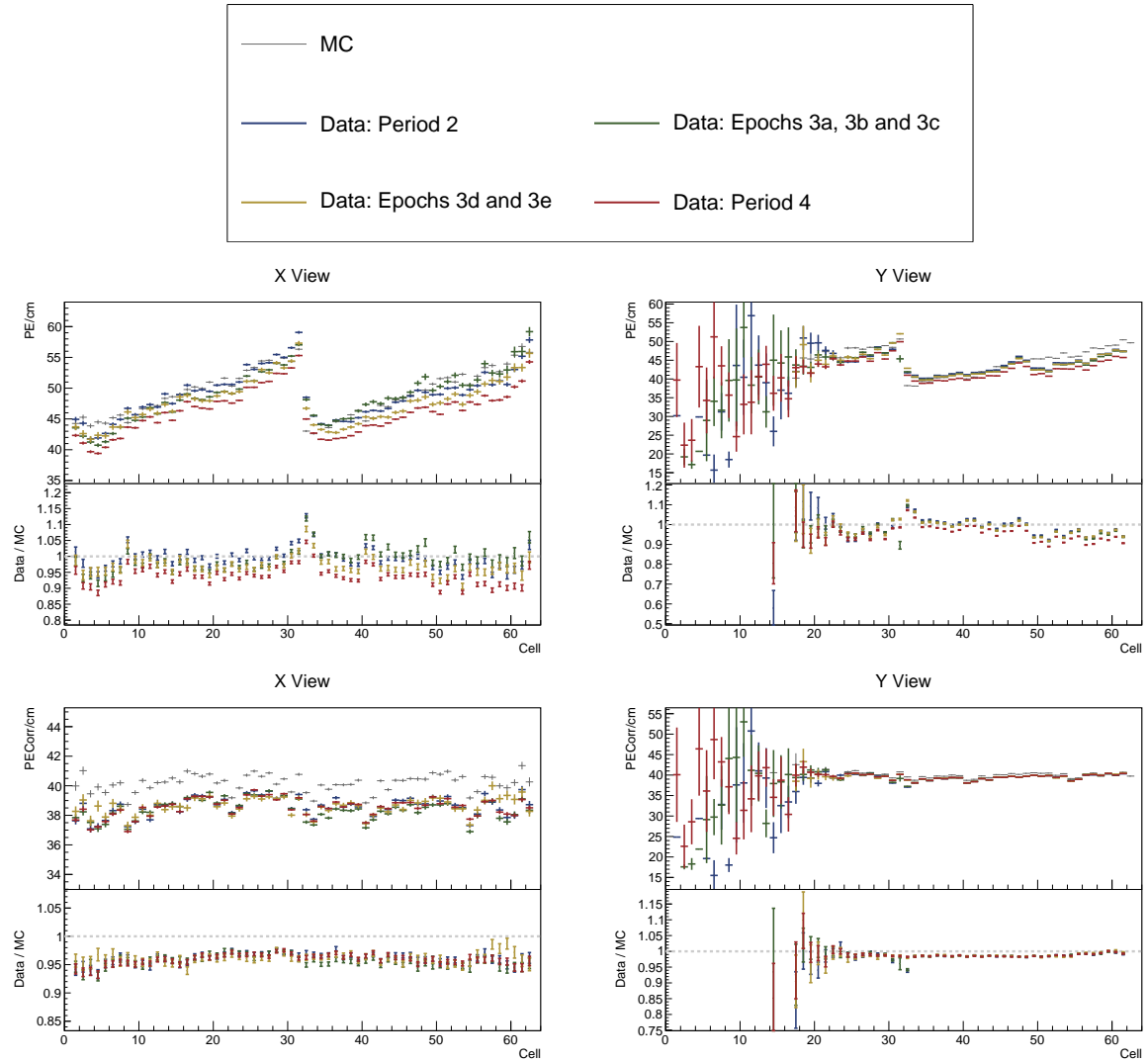


Figure 28: ...

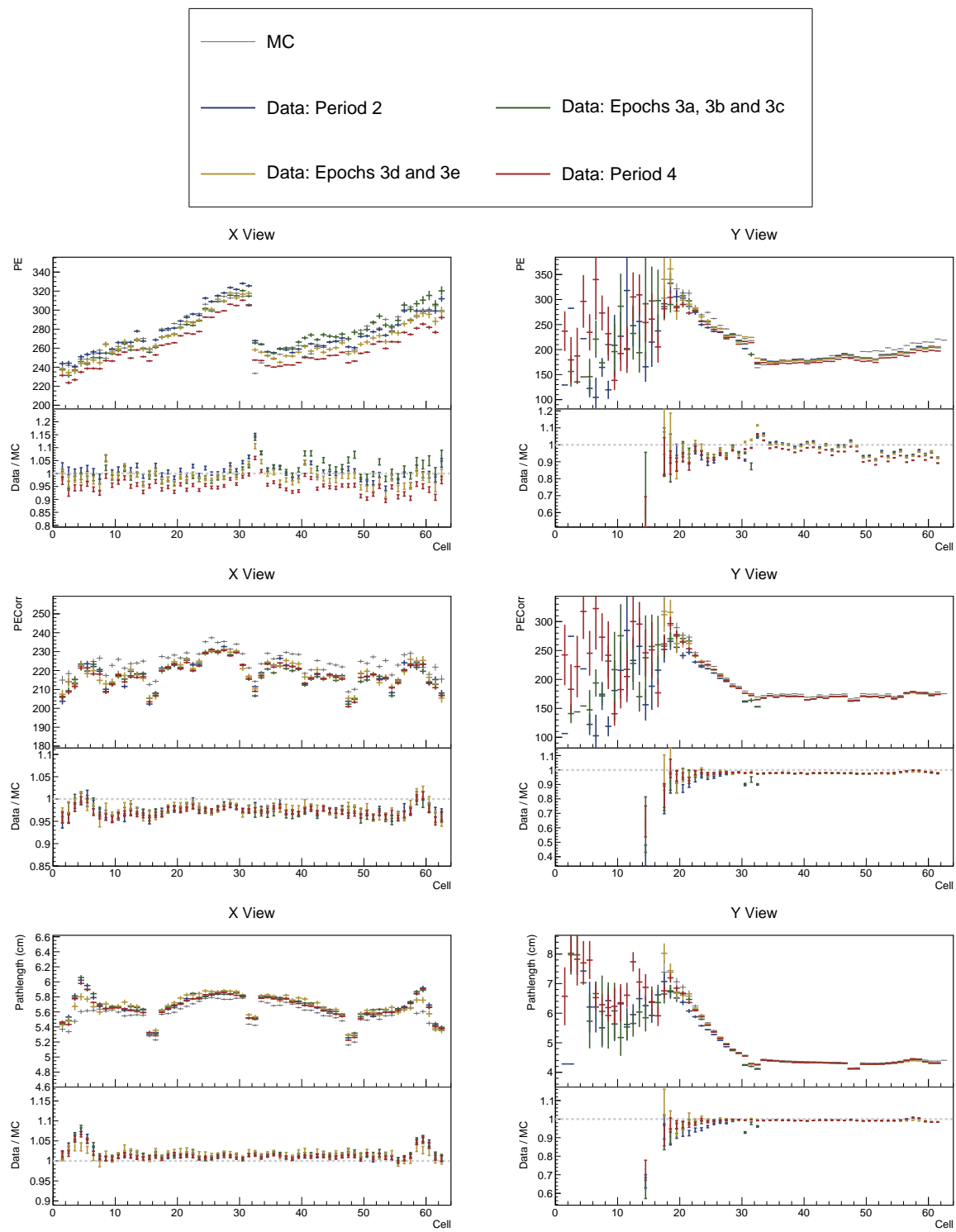


Figure 29: ...

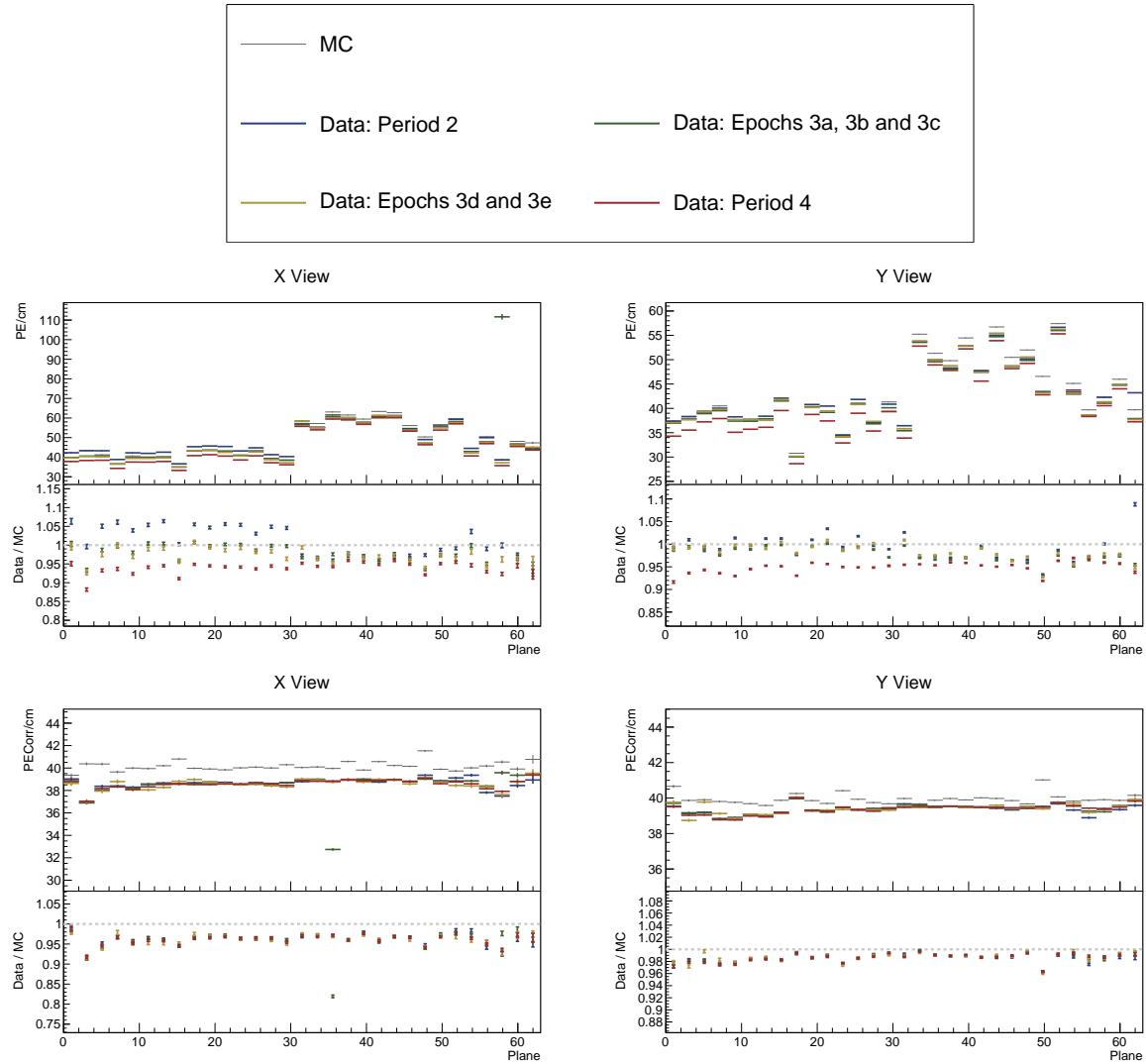


Figure 30: ...

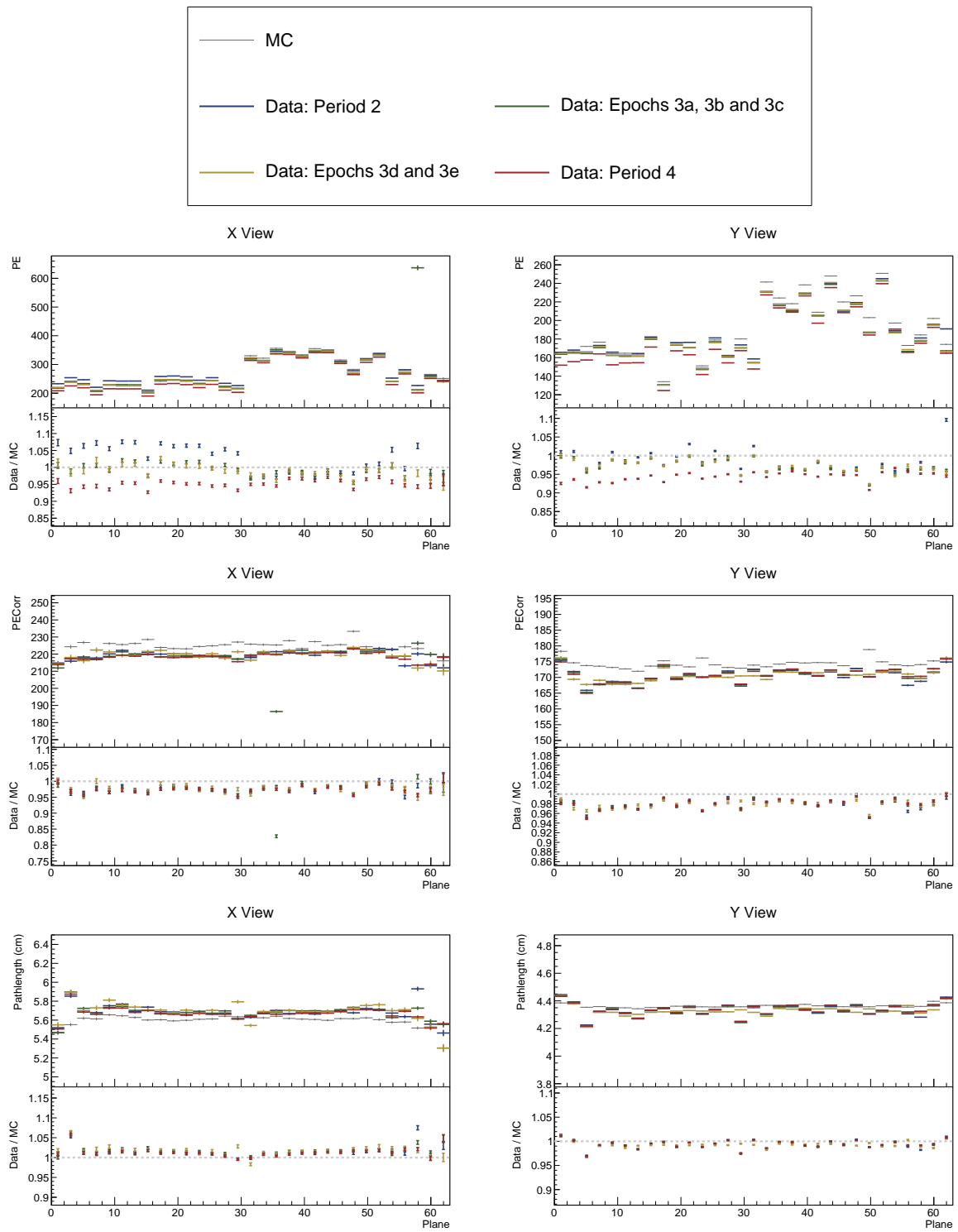


Figure 31: ...

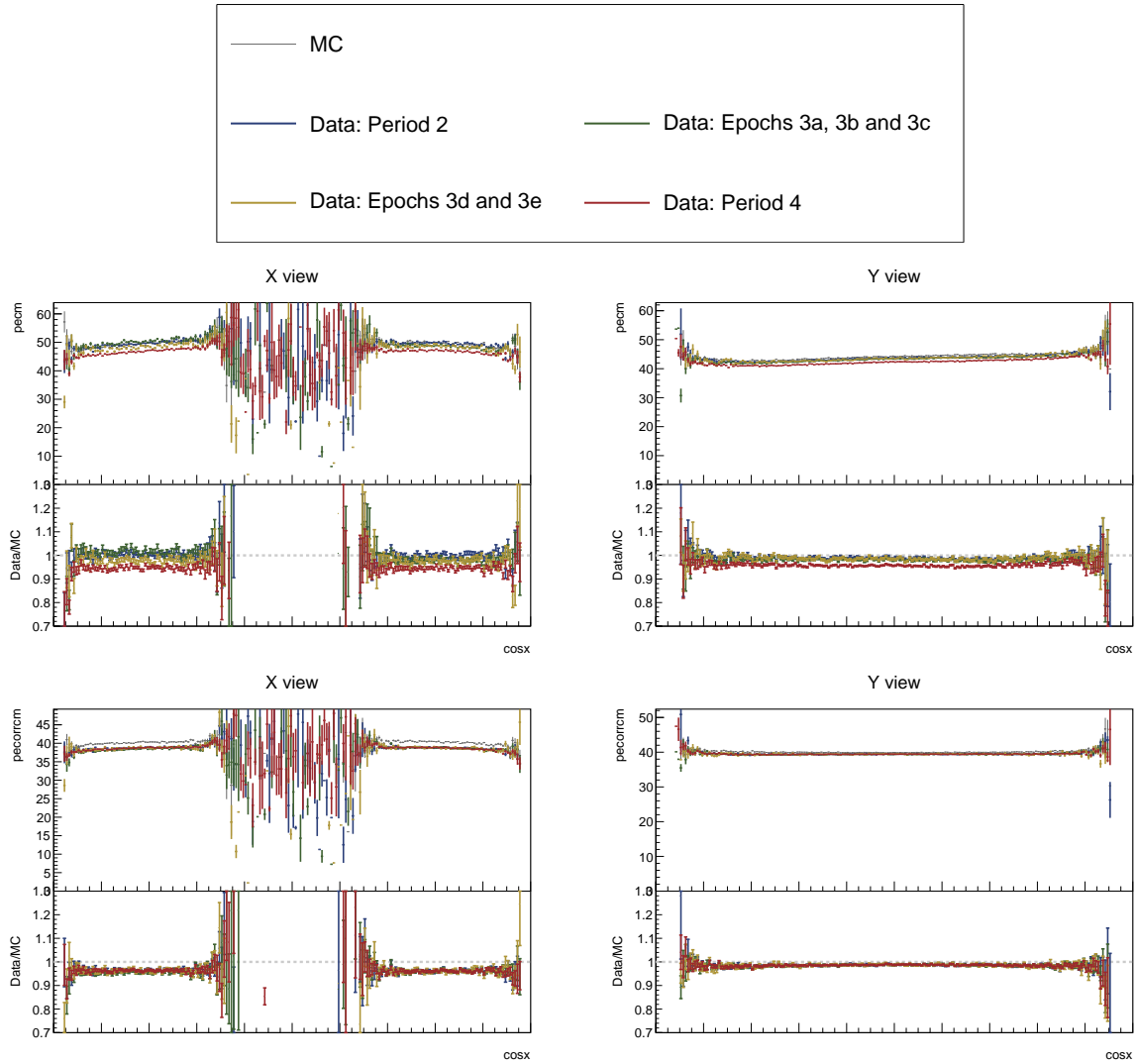


Figure 32: ...

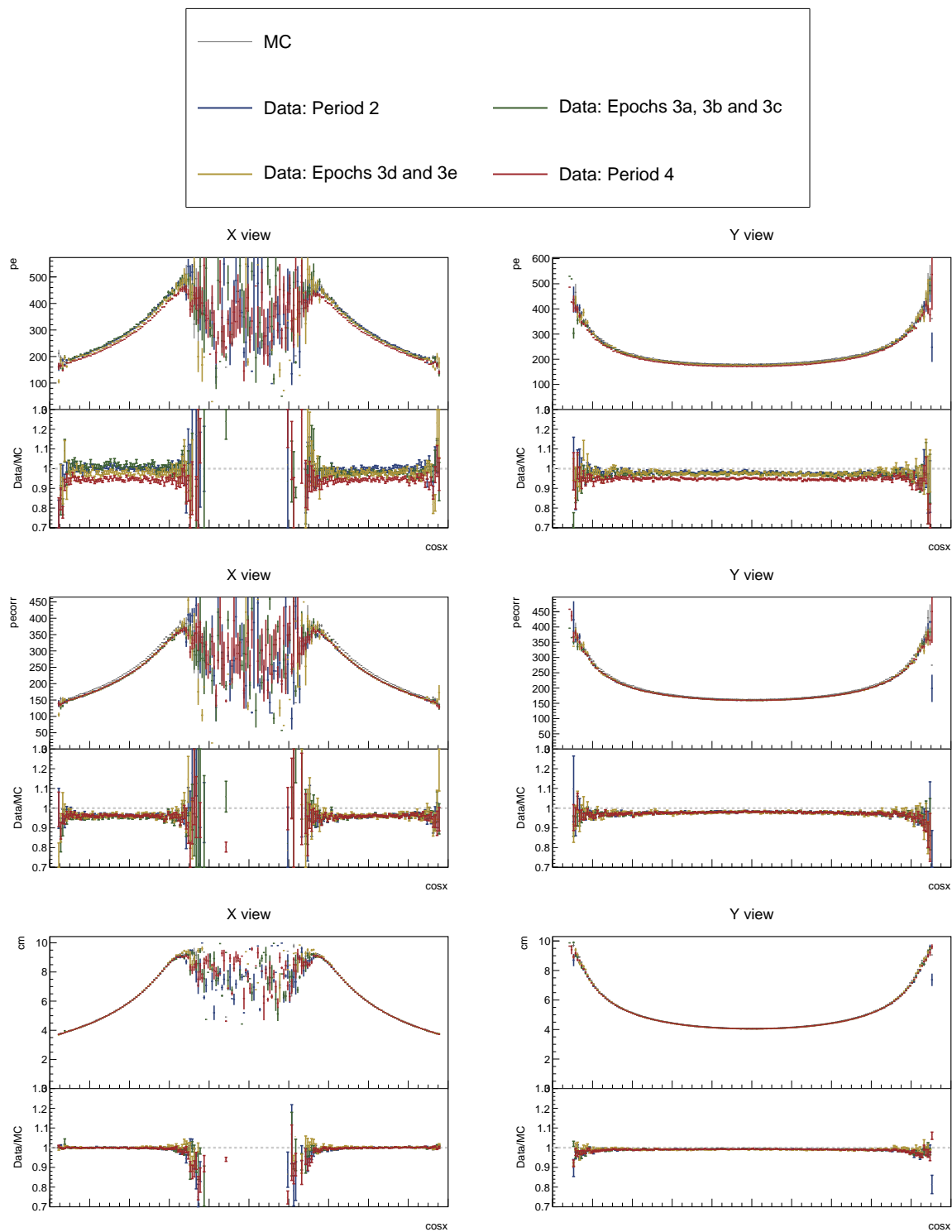


Figure 33: ...

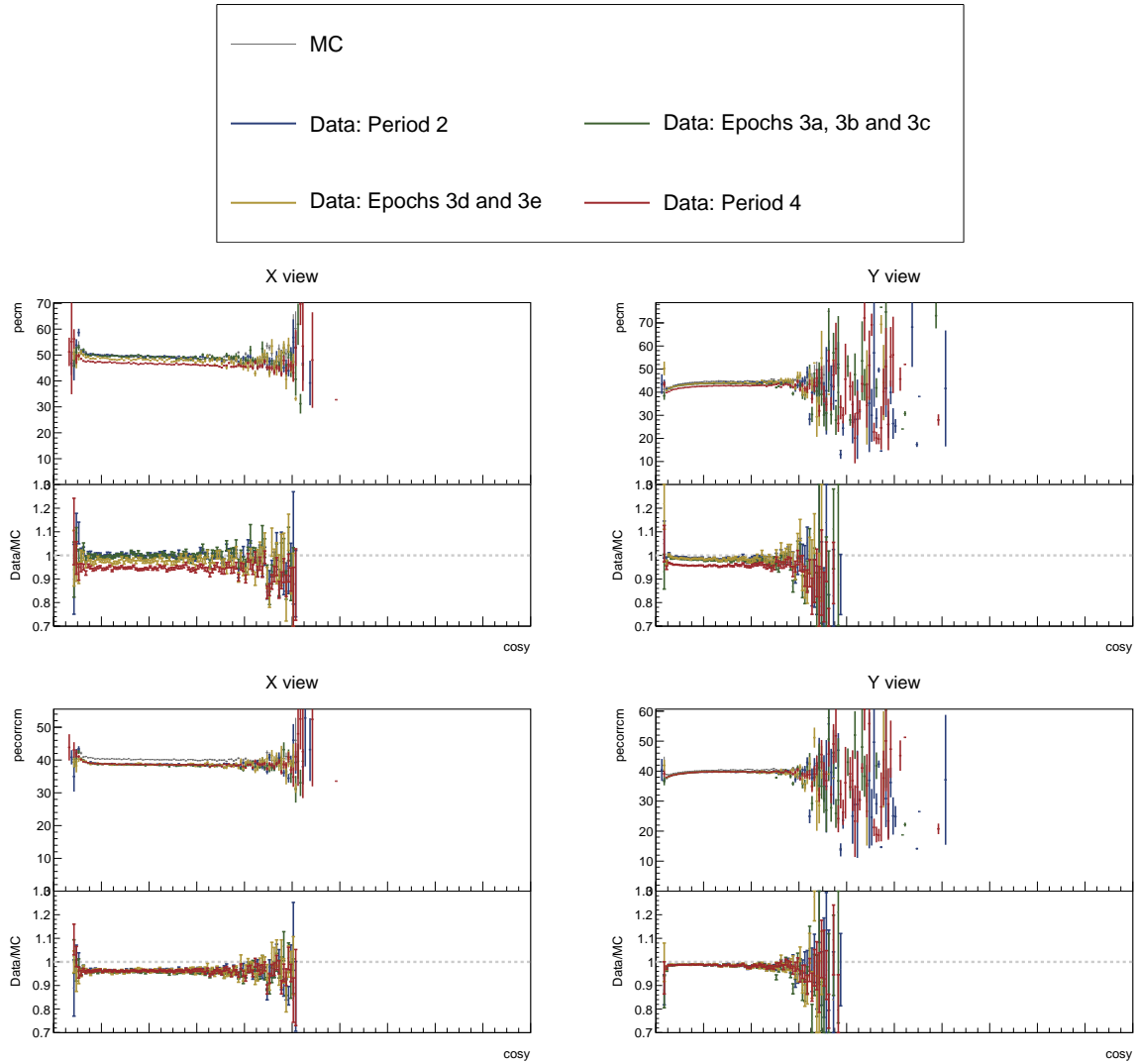


Figure 34: ...

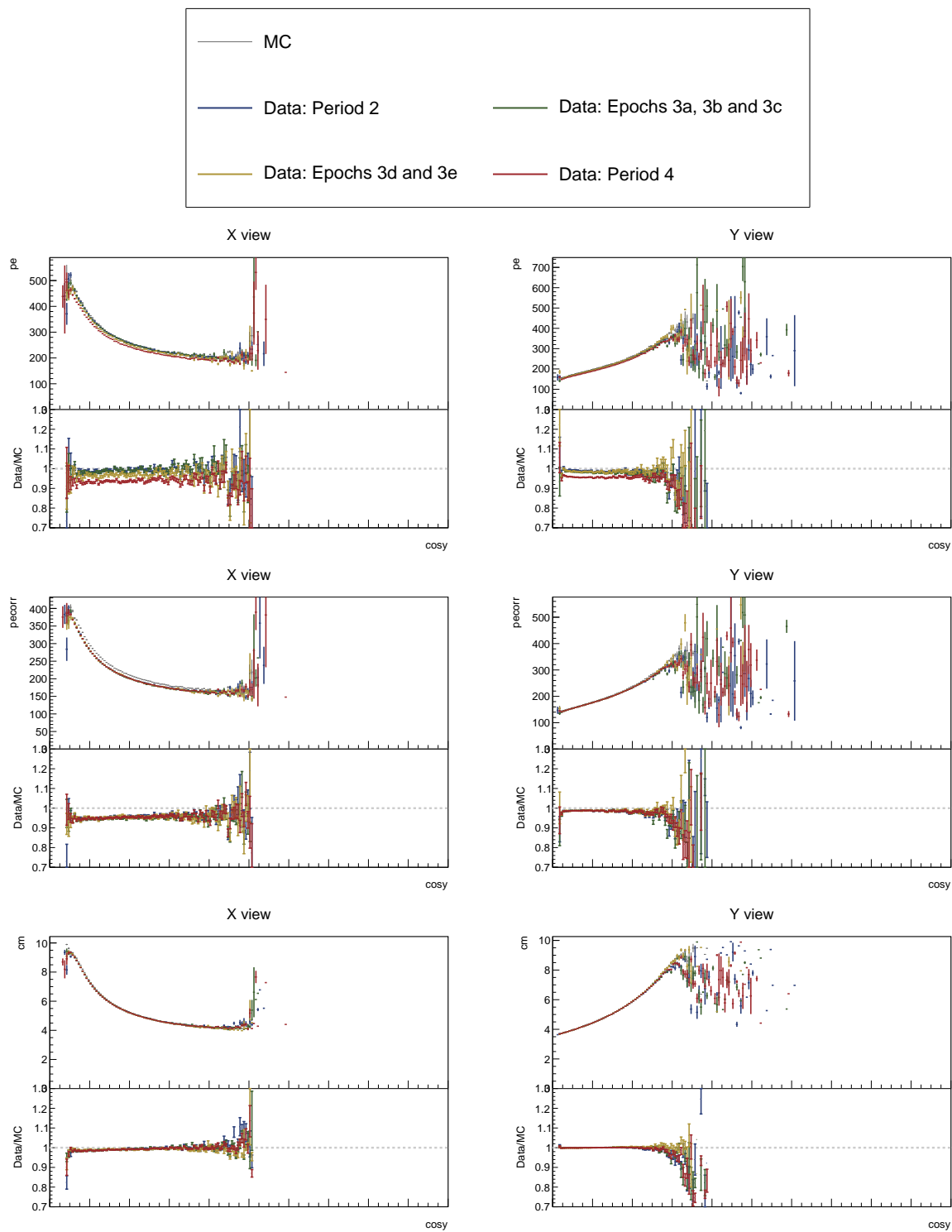


Figure 35: ...

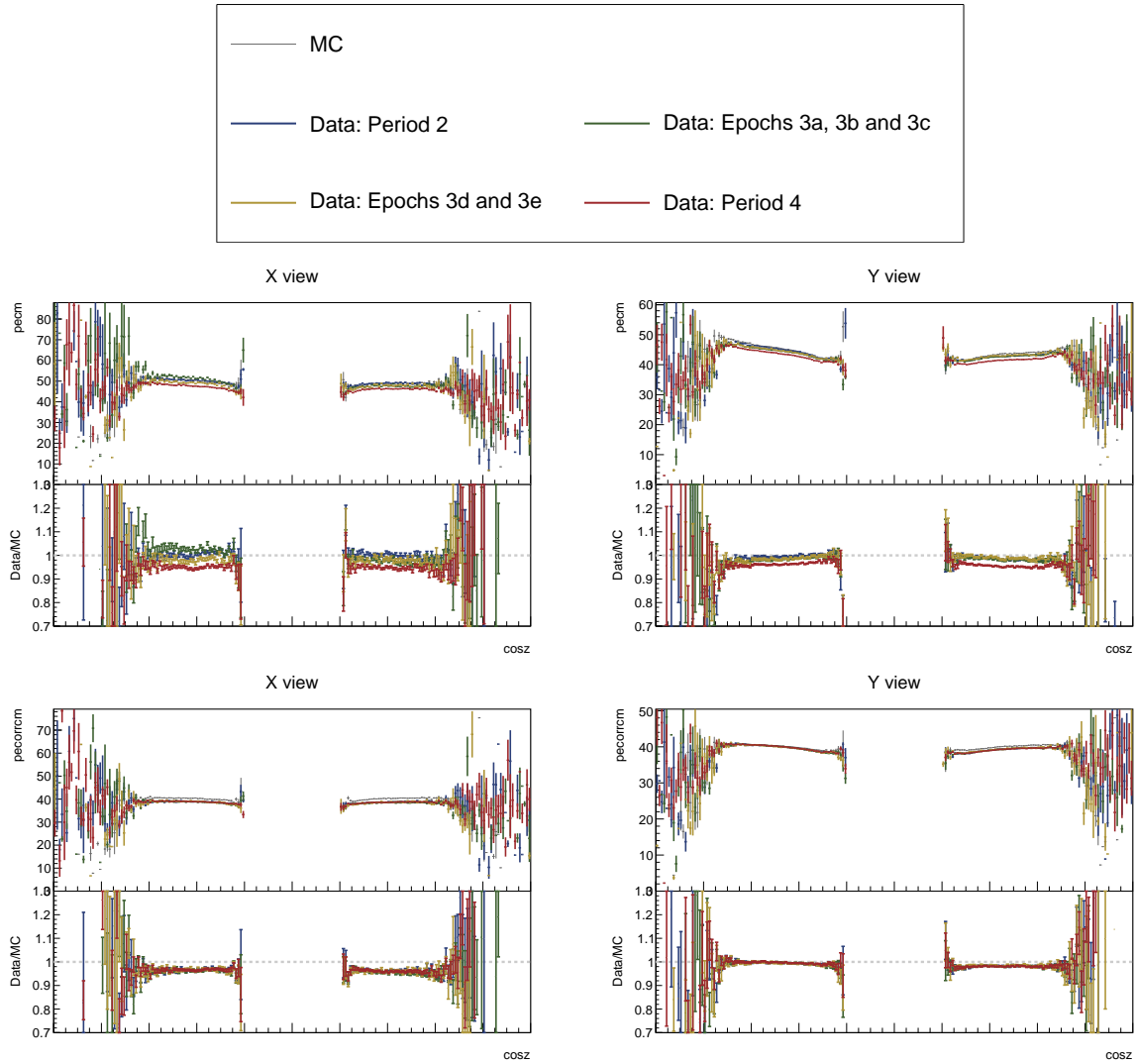


Figure 36: ...

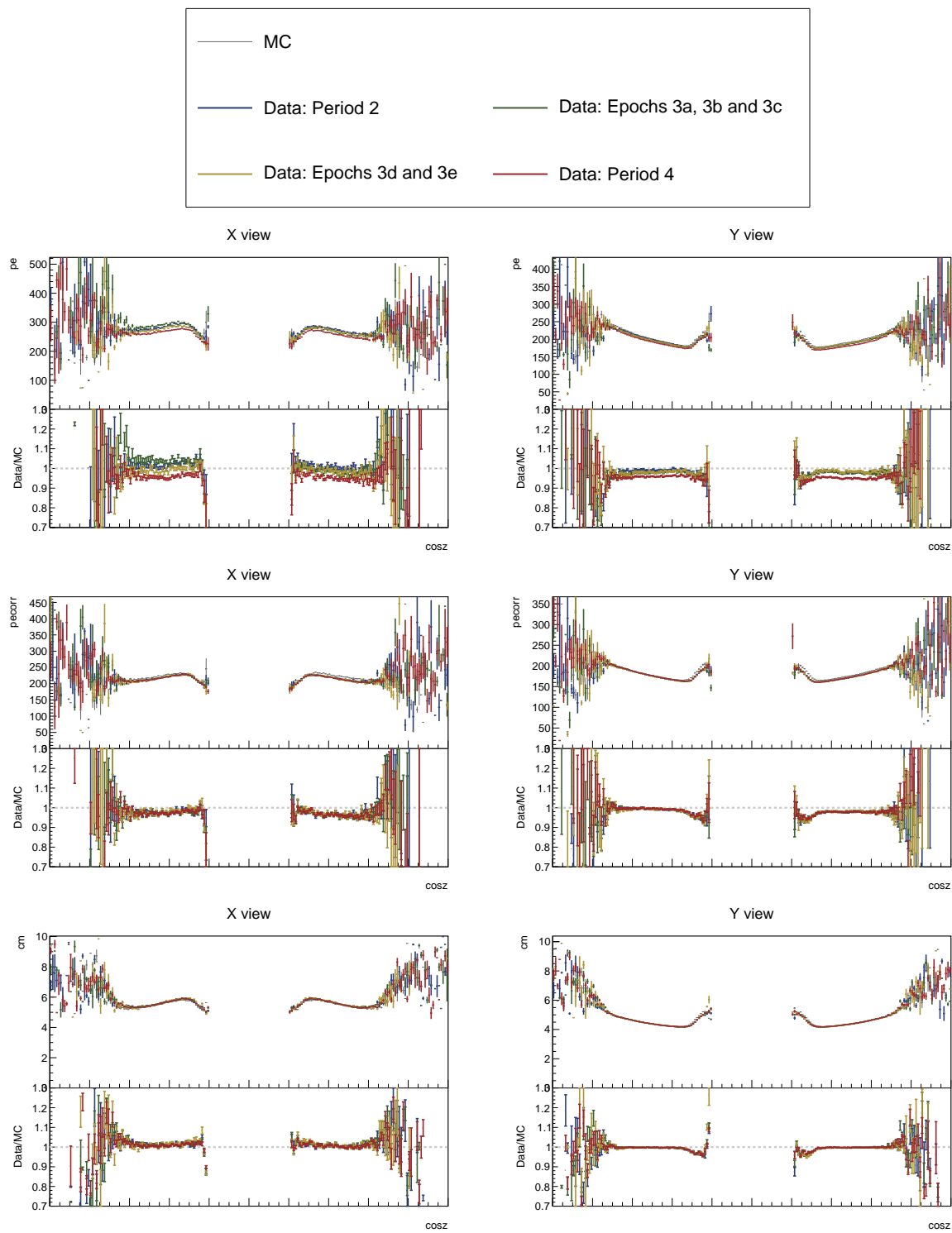


Figure 37: ...

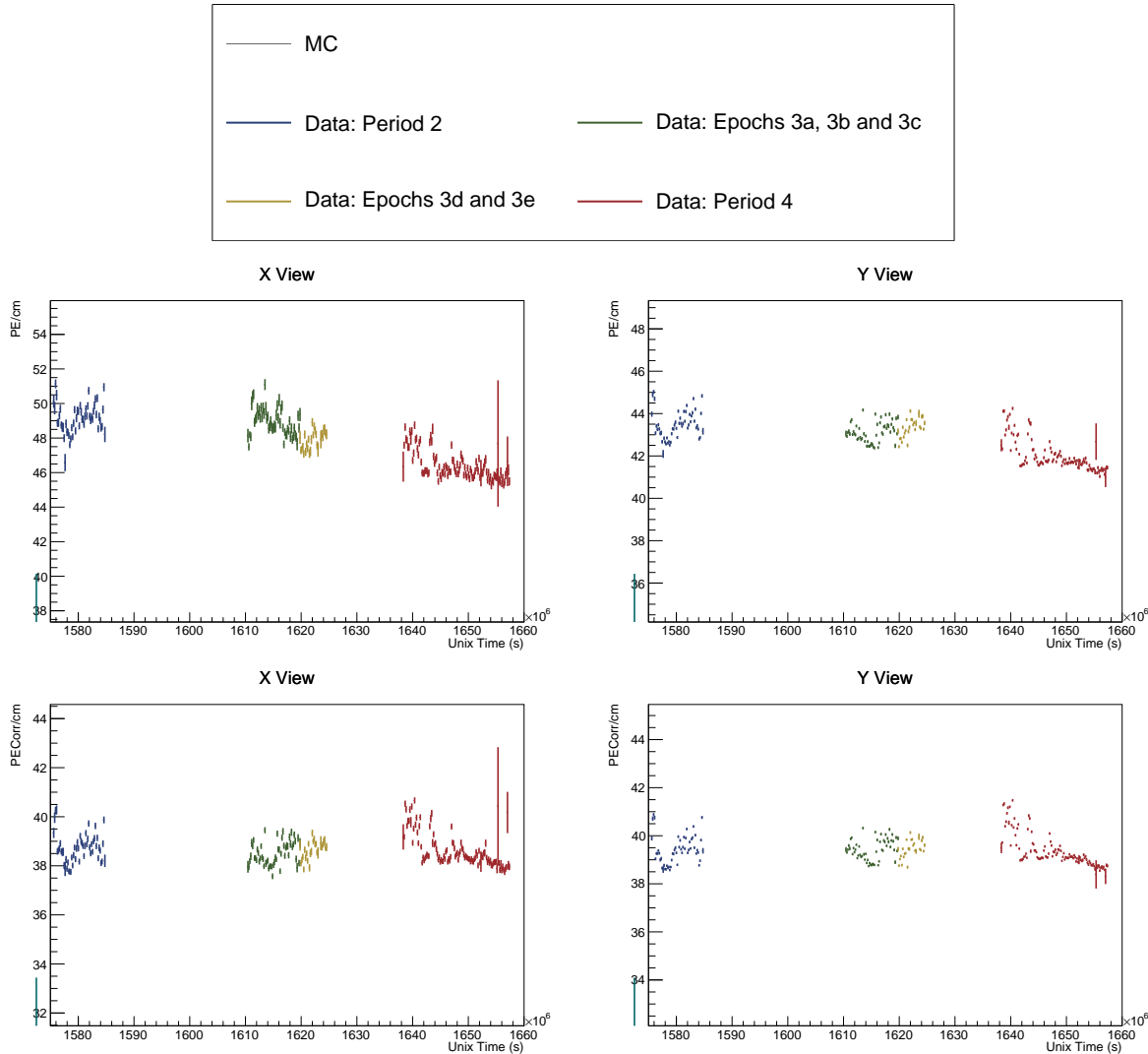


Figure 38: ...

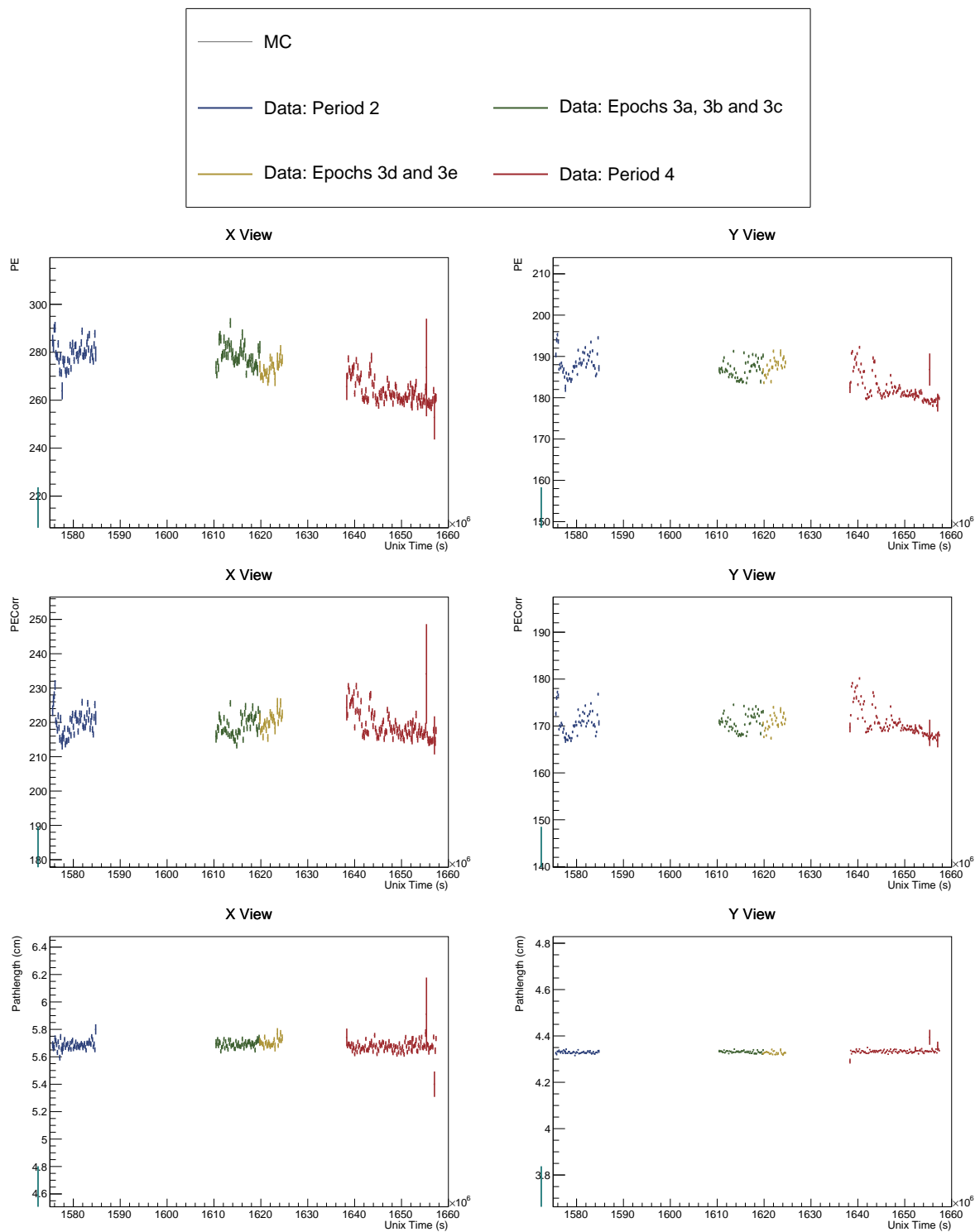


Figure 39: ...